Supplementary Information for

Colony formation sustains the global competitiveness of N_2-fixing *Trichodesmium* under ocean acidification

Weicheng Luo[1, 2, 3], Meri Eichner[2], Ondřej Prášil[2], Keisuke Inomura[4], Futing Zhang[2], Ya-Wei Luo[1, 5]*

[1]State Key Laboratory of Marine Environmental Science and College of Ocean and Earth Sciences, Xiamen University, Xiamen 361102, China.

[2]Centre Algatech, Institute of Microbiology of the Czech Academy of Sciences, Třeboň 37901, Czech Republic.

[3]Institute for Advanced Study, Shenzhen University, Shenzhen 518060, China. & College of Life Sciences and Oceanography, Shenzhen University, Shenzhen 518060, China.

[4]Graduate School of Oceanography, University of Rhode Island, Narragansett, RI 02882, USA.

[5]China-ASEAN College of Marine Sciences, Xiamen University Malaysia, Sepang, Selangor 43900, Malaysia

*To whom correspondence should be addressed. Email: ywluo@xmu.edu.cn (Y-W.L.)

Supplementary Table 1. Daily average rates in modeled *Trichodesmium* trichome and colony. *Related to Fig. 2.*

Model cases	Growth (d^{-1})	Gross carbon fixation [mol C (mol C)$^{-1}$ d^{-1}]	N_2 fixation [mol N (mol C)$^{-1}$ d^{-1}]	Gross fixed C:N [mol C (mol N)$^{-1}$]	Gross fixed carbon used by respiratory protection	Carbon use efficiency [a]
Trichome (Limiting Fe′ = 40 pM)						
Ambient	0.24	3.2	0.044	74	88%	8.5%
OA	0.18	2.9	0.032	89	89%	7.0%
Trichome (Replete Fe′ = 1250 pM)						
Ambient	0.42	3.8	0.082	47	81%	13.5%
OA	0.33	3.5	0.061	58	83%	10.9%
Colony (Limiting Fe′ = 40 pM)						
Ambient	0.20	3.1	0.036	85	89%	7.4%
OA	0.17	2.9	0.029	99	90%	6.4%
Colony (Replete Fe′ = 1250 pM)						
Ambient	0.35	3.6	0.068	53	83%	11.8%
OA	0.30	3.5	0.056	63	85%	10.0%

[a] Carbon use efficiency: percentage of gross carbon fixation assimilated to biomass. OA: acidified condition.

Supplementary Table 2. Comparison of simulated acidification-induced effects on N_2 fixation from between this study and Luo, et al. [1]. *Related to Fig. 5 and DISCUSSION.*

Acidification-induced effects on N_2 fixation [a]	**Luo, et al.** [1]	**This study**
Energy saving from CCM	< 1%	< 1%
Downregulation on nitrogenase efficiency	about -40%	about -40%
Reduced energy production by PET or elevated energy consumption	about -10%	about -10%
Intracellular O_2 management	Not considered	about -5%

[a] Model results under Fe limitation were analyzed here.

Supplementary Table 3. Modeled daily-integrated rates of *Trichodesmium* colony with toxicity effects. *Related to Fig. 6 and DISCUSSION.*

Model cases [a]	Growth rate (d^{-1})	Gross carbon fixation rate [mol C (mol C)$^{-1}$ d^{-1}]	N_2 fixation rate [mol N (mol C)$^{-1}$ d^{-1}]	Gross fixed C:N [mol C (mol N)$^{-1}$]	Gross fixed carbon used by respiratory protection	Carbon use efficiency
			Colony (Fe′ = 40 pM)			
Ambient	0.09	2.2	0.015	147	93.8%	4.3%
Acidified	0.11	2.5	0.018	139	93.1%	4.5%
			Colony (Fe′ = 1250 pM)			
Ambient	0.17	2.4	0.030	82	88.9%	7.7%
Acidified	0.20	3.0	0.034	87	88.9%	7.2%

[a] Microenvironmental NH_4^+ concentration profile was predefined according to the findings of Klawonn, et al. [2]. The pattern of microenvironmental Cu was set the same as that of NH_4^+, with the highest concentration (1 nmol L^{-1}) at the center of the colony. The elevated iron acquisition due to colony formation under the acidified condition was not taken into consideration here.

Supplementary Table 4. Fixed model parameters. *Related to METHODS.*

Symbol	Unit	Definition	Value	Source or note
OA^{PET}	dimensionless	Parameter of OA impact on the ATP production by PET	0.4	This study [a]
OA^{RESP}	dimensionless	Parameter of OA impact on the ATP production by respiration	0.4	This study [a]
ε_{CO_2}	dimensionless	Relative CO_2 diffusivity of cell membrane	1.5×10^{-3}	This study [a]
f_{RP}^{CF}	dimensionless	Fraction of CO_2 production by RP to support carbon fixation	75%	This study [a]
N_{max}	mol N (mol C)$^{-1}$	Maximal fixed storage	0.159	This study [b]
CS_{max}	mol C (mol C)$^{-1}$	Maximal CS storage	1	This study [c]
k_{NH_3}	mol N m^{-3}	Half-saturating coefficient of NH_3 concentration for the toxic effect	3×10^{-5}	This study [d]
k_{Cu}	mol Cu m^{-3}	Half-saturating coefficient of Cu concentration for the toxic effect	2.5×10^{-7}	This study [d]
OA^{Cu}	dimensionless	Strength of negative effects from acidification on copper availability	1.65	This study [d]
v_{CS}^{max}	mol C (mol C)$^{-1}$ s^{-1}	Maximal production rate of CS	8.6×10^{-6}	[3]
k_{CS}	mol C (mol C)$^{-1}$	Half-saturating coefficient of CS for RP	0.4	[3]
$k_{CH_2O}^{CS}$	mol C (mol C)$^{-1}$	Half-saturating coefficient of CH_2O for CS production	0.4	[3]
v_{PET}^{max}	mol electron (mol C)$^{-1}$ s^{-1}	Maximal PET rate	6.6×10^{-3}	[3]
k_{Fe}^{PS}	μmol Fe (mol C)$^{-1}$	Half-saturating coefficient of Fe in photosystems for PET rate	10	[3]
$k_{Fe_{PS}}^{PS_{syn}}$	μmol Fe (mol C)$^{-1}$	Half-saturating coefficient of Fe_{PS} for the synthesis of photosystems	1.0	[3]
$k_{Fe_{PS}}^{PS_{dec}}$	μmol Fe (mol C)$^{-1}$	Half-saturating coefficient of Fe_{PS} for the decomposition of photosystems	25	[3]
$k_{Fe_{BF}}^{NF_{syn}}$	μmol Fe (mol C)$^{-1}$	Half-saturating coefficient of Fe_{BF} for the synthesis of nitrogenase	5.0	[3]
$T_{NF_{max}}^{NA}$	μmol Fe (mol C)$^{-1}$	Maximal inactivation rate of nitrogenase	3.3×10^{-3}	[3]
k_{Fe}^{NF}	μmol Fe (mol C)$^{-1}$	Half-saturating coefficient of Fe in nitrogenase for N_2 fixation	91	[1]
$k_{O_2}^{NF}$	mol O_2 m^{-3}	Half-saturating coefficient of O_2 for N_2 fixation	0.01	[4]
Fe_{TH}^{bsl}	μmol Fe (mol C)$^{-1}$	Threshold of Fe under the baseline condition	24.4	[1]
f_{ST}	dimensionless	Fraction of luxury Fe uptake	0.90	[1]
OA^{ST}	dimensionless	Coefficient representing the strength of OA impact on Fe_{TH}	0.71	[1]
α_I	μmol^{-1} m^2 s	Initial slope of *P* versus *I* curve	0.01	[5]
β	(mol C)$^{-1}$ mol C s	Parameter of inhibition effect of respiration on PET	2×10^4	[4]
ε	dimensionless	Relative O_2 diffusivity of cell membrane	10^{-4}	[4]
d_{O_2}	m^2 s^{-1}	O_2 diffusion coefficient at 34 PSU and 25 °C	2.26×10^{-9}	[6]
d_{CO_2}	m^2 s^{-1}	CO_2 diffusion coefficient at 34 PSU and 25 °C	1.79×10^{-9}	[7]
γ_{MT}	dimensionless	Ratio of the energy consumed by maintenance to other process	10%	[1]
		Additional parameters for colony		
RC	m	Radius of the colony	8×10^{-4}	[2]
$d_{HCO_3^-}$	m^2 s^{-1}	HCO_3^- diffusion coefficient at 34 PSU and 25 °C	1.10×10^{-9}	[7]
$d_{CO_3^{2-}}$	m^2 s^{-1}	CO_3^{2-} diffusion coefficient at 34 PSU and 25 °C	9.28×10^{-10}	[7]
d_{H^+}	m^2 s^{-1}	H^+ diffusion coefficient at 34 PSU and 25 °C	8.68×10^{-9}	[7]
d_{OH^-}	m^2 s^{-1}	OH^- diffusion coefficient at 34 PSU and 25 °C	4.91×10^{-9}	[7]
k_{+1}	s^{-1}	Forward rate coefficient of $CO_2 + H_2O \underset{k_{-1}}{\overset{k_{+1}}{\rightleftharpoons}} HCO_3^- + H^+$	3.60×10^{-2}	[7]
k_{-1}	m^3 mol^{-1} s^{-1}	Reverse rate coefficient of $CO_2 + H_2O \underset{k_{-1}}{\overset{k_{+1}}{\rightleftharpoons}} HCO_3^- + H^+$	32.2	[7]
k_{+4}	m^3 mol^{-1} s^{-1}	Forward rate coefficient of $CO_2 + OH^- \underset{k_{-4}}{\overset{k_{+4}}{\rightleftharpoons}} HCO_3^-$	8.28	[7]
k_{-4}	s^{-1}	Reverse rate coefficient of $CO_2 + OH^- \underset{k_{-4}}{\overset{k_{+4}}{\rightleftharpoons}} HCO_3^-$	3.70×10^{-4}	[7]

k_{+5}	$m^3\ mol^{-1}\ s^{-1}$	Forward rate coefficient of $CO_3^{2-} + H^+ \underset{k_{-5}}{\overset{k_{+5}}{\rightleftarrows}} HCO_3^-$	9.75×10^6	7
k_{-5}	s^{-1}	Reverse rate coefficient of $CO_3^{2-} + H^+ \underset{k_{-5}}{\overset{k_{+5}}{\rightleftarrows}} HCO_3^-$	9.00	7
k_{+6}	$m^3\ mol^{-1}\ s^{-1}$	Forward rate coefficient of $H_2O \underset{k_{-6}}{\overset{k_{+6}}{\rightleftarrows}} H^+ + OH^-$	1.33	7
k_{-6}	$m^3\ mol^{-1}\ s^{-1}$	Reverse rate coefficient of $H_2O \underset{k_{-6}}{\overset{k_{+6}}{\rightleftarrows}} H^+ + OH^-$	2.67×10^7	7
		Boundary conditions		
I_{max}	$\mu mol\ m^{-2}\ s^{-1}$	Maximal light intensity in fixed-Fe and dynamic-Fe cases under diurnally changing light intensity	160	
O_2^E	mol O_2 m^{-3}	Extracellular far-field O_2	0.213	
$CO_{2,\ bsl}^E$	mol C m^{-3}	Extracellular far-field CO_2	0.014	
$HCO_{3,\ bsl}^E$	mol C m^{-3}	Extracellular far-field HCO_3^-	1.87	
pH_{bsl}	dimensionless	pH value under baseline condition	8.08	
		Elemental or energy stoichiometries of metabolic activities		
q_{LPET}^{NADPH}	mol NADPH (mol electron)$^{-1}$	NADPH/electron ratio of LPET	0.5	8
q_{LPET}^{ATP}	mol ATP (mol electron)$^{-1}$	ATP/electron ratio of LPET	0.65	9
$q_{LPET}^{O_2}$	mol O_2 (mol electron)$^{-1}$	O_2/electron ratio of LPET	0.25	8
q_{AET}^{ATP}	mol ATP (mol electron)$^{-1}$	ATP/electron ratio of MR-AET	0.65	9
q_{NF}^{NADPH}	mol NADPH (mol N)$^{-1}$	NADPH/N ratio of N_2 fixation	3	10,11
q_{NF}^{ATP}	mol ATP (mol N)$^{-1}$	ATP/N ratio of N_2 fixation	9	10,11
q_{CF}^{NADPH}	mol NADPH (mol C)$^{-1}$	NADPH/C ratio of C fixation	2	12
q_{CF}^{ATP}	mol ATP (mol C)$^{-1}$	ATP/C ratio of C fixation	3	12
$q_{HCO_3^-}^{ATP}$	mol ATP (mol C)$^{-1}$	ATP/C ratio of CCM for per HCO_3^- transportation	0.5	13
q_{BIO}^{ATP}	mol ATP (mol C)$^{-1}$	ATP/C ratio of biosynthesis	2	5
q_{RESP}^{ATP}	mol ATP (mol C)$^{-1}$	ATP/C ratio of respiration	5	14
$q_C^{O_2}$	mol O_2 (mol C)$^{-1}$	O_2/C ratio of respiration	1	14
Q_C	mol C m^{-3}	Cellular carbon biomass concentration	18333	15
		Morphological parameters of Trichodesmium		
L	m	Length of the total trichome	554×10^{-6}	16
R	m	Radius of the cytoplasm	4.80×10^{-6}	16
L_g	m	Thickness of cell membrane layer	0.076	16

[a] Estimated based on model experiments under constant light intensity.

[b] By multiplying the initial C biomass with the molar N:C (0.159) of *Trichodesmium* [17].

[c] CS_{max} is set to be the same as the initial C biomass.

[d] Estimated based on model experiments with toxicity effects.

Supplementary Table 5. Optimized parameters under dynamic light intensity. *Related to METHODS.*

Symbol	Unit	Definition	Conditions of Fe level	Value			
				Trichome		Colony	
				Ambient	Acidified	Ambient	Acidified
v_{RP}^{max}	mol C (mol C)$^{-1}$ s^{-1}	Maximal respiratory protection rate	High Fe	1.3×10^{-3}	1.3×10^{-3}	1.2×10^{-3}	1.4×10^{-3}
			Low Fe	1.4×10^{-3}	1.2×10^{-3}	1.3×10^{-3}	1.4×10^{-3}
$T_{PS_{max}}^{BF}$	μmol Fe (mol C)$^{-1}$ s^{-1}	Maximal synthesis rate of photosystems	High Fe	2.3×10^{-6}	1.3×10^{-7}	2.3×10^{-6}	1.3×10^{-7}
			Low Fe	1.3×10^{-9}	6.2×10^{-9}	1.3×10^{-9}	6.2×10^{-9}
$T_{BF_{max}}^{PS}$	μmol Fe (mol C)$^{-1}$ s^{-1}	Maximal decomposition rate of photosystems	High Fe	3.1×10^{-3}	3.9×10^{-4}	3.1×10^{-3}	3.9×10^{-4}
			Low Fe	1.2×10^{-3}	1.2×10^{-4}	1.2×10^{-3}	1.2×10^{-4}
$T_{NF_{max}}^{BF}$	μmol Fe (mol C)$^{-1}$ s^{-1}	Maximal synthesis rate of photosystems	High Fe	2.8×10^{-2}	2.7×10^{-2}	2.8×10^{-2}	2.7×10^{-2}
			Low Fe	2.8×10^{-2}	2.6×10^{-2}	2.8×10^{-2}	2.1×10^{-2}

Supplementary Table 6. Intermediate process variables. *Related to METHODS.*

Symbol	Unit	Definition
I	μmol m^{-2} s^{-1}	Daytime light intensity
V_{PET}	mol electron (mol C)$^{-1}$ s^{-1}	PET rate
V_{LPET}	mol electron (mol C)$^{-1}$ s^{-1}	LPET rate
V_{AET}	mol electron (mol C)$^{-1}$ s^{-1}	AET rate
f_{AET}	dimensionless	Fraction of electrons in PET to AET
V_{NAPDH}	mol NADPH (mol C)$^{-1}$ s^{-1}	NADPH production rate
V_{ATP}	mol ATP (mol C)$^{-1}$ s^{-1}	ATP production rate
V_{O_2}	mol O_2 (mol C)$^{-1}$ s^{-1}	O_2 production rate
V_{NF}^{max}	mol N (mol C)$^{-1}$ s^{-1}	Maximal N_2 fixation rate
V_{NF}	mol N (mol C)$^{-1}$ s^{-1}	N_2 fixation rate
Φ	dimensionless	Intracellular requirement of N_2 fixation
V_{NF}^{CCM}	mol N (mol C)$^{-1}$ s^{-1}	N_2 fixation rate supported by energy saving from CCM
V_{NADPH}^{NF}	mol NADPH (mol C)$^{-1}$ s^{-1}	NADPH consumption rate of N_2 fixation
V_{ATP}^{NF}	mol ATP (mol C)$^{-1}$ s^{-1}	ATP consumption rate of N_2 fixation
q_{CCM}^{ATP}	mol ATP (mol C)$^{-1}$	Energy cost for per DIC transportation of CCM
V_{ATP}^{CCM}	mol ATP (mol C)$^{-1}$ s^{-1}	ATP consumption rate of CCM
$V_{ATP}^{CCM,\ saving}$	mol ATP (mol C)$^{-1}$ s^{-1}	Rate of energy saving by CCM
V_{NADPH}^{CF}	mol NADPH (mol C)$^{-1}$ s^{-1}	NADPH consumption rate of C fixation
V_{ATP}^{CF}	mol ATP (mol C)$^{-1}$ s^{-1}	ATP consumption rate of C fixation
V_{CS}	mol C (mol C)$^{-1}$ s^{-1}	Carbon skeleton production rate
V_{RP}	mol C (mol C)$^{-1}$ s^{-1}	Respiratory protection rate
$V_{O_2}^{RP}$	mol O_2 (mol C)$^{-1}$ s^{-1}	O_2 consumption rates by respiratory protection
T_{O_2}	mol O_2 m^{-3} s^{-1}	O_2 diffusion rate between cytoplasm and far-field environment
T_{CO_2}	mol CO_2 m^{-3} s^{-1}	CO_2 diffusion rate between cytoplasm and far-field environment
Fe_{TH}	μmol Fe (mol C)$^{-1}$	Threshold of intracellular metabolic Fe quota
Fe_M	μmol Fe (mol C)$^{-1}$	Intracellular Fe quota in metabolism
Fe_{ST}	μmol Fe (mol C)$^{-1}$	Intracellular Fe quota in storage
T_{PS}^{BF}	μmol Fe (mol C)$^{-1}$ s^{-1}	Synthesis rate of photosystems
T_{BF}^{PS}	μmol Fe (mol C)$^{-1}$ s^{-1}	Decomposition rate of photosystems
T_{NF}^{BF}	μmol Fe (mol C)$^{-1}$ s^{-1}	Synthesis rate of nitrogenase
T_{NF}^{NA}	μmol Fe (mol C)$^{-1}$ s^{-1}	Inactivation rate of nitrogenase
Bio	mol C (mol C)$^{-1}$	New synthesized biomass
Bio_N	mol C (mol C)$^{-1}$	New synthesized N-based biomass
Bio_C	mol C (mol C)$^{-1}$	New synthesized C-based biomass
$CH_2O_{BIO}^{RESP}$	mol C (mol C)$^{-1}$	Respired carbohydrates to fulfill the energy need for biosynthesis
G	d^{-1}	Specific growth rate
	Additional intermediate process variables of colony	
ψ	dimensionless	Porosity of colony
η	dimensionless	DIC limitation effect on CF
ξ	dimensionless	Toxicity effects of NH_3 and/or Cu
$J_{CO_2^M}$	mol C m^{-3} s^{-1}	Change rates of CO_2 driven by the chemical reactions in carbonate systems
$J_{HCO_3^M}$	mol C m^{-3} s^{-1}	Change rates of HCO_3^- driven by the chemical reactions in carbonate systems
$J_{CO_3^M}$	mol C m^{-3} s^{-1}	Change rates of CO_3^{2-} driven by the chemical reactions in carbonate systems
J_{H^M}	mol H^+ m^{-3} s^{-1}	Change rates of H^+ driven by the chemical reactions in carbonate systems
J_{OH^M}	mol OH^- m^{-3} s^{-1}	Change rates of OH^- driven by the chemical reactions in carbonate systems
$T_{C,\ O_2}^M$	mol O_2 m^{-3} s^{-1}	O_2 diffusion rate between the intracellular cytoplasm and the extracellular microenvironment
$T_{C,\ CO_2}^M$	mol C m^{-3} s^{-1}	Net biological consumption rates of CO_2 of colony
$T_{C,\ HCO_3^-}^M$	mol C m^{-3} s^{-1}	Net biological consumption rates of HCO_3^- of colony
$T_{C,\ H}^M$	mol H^+ m^{-3} s^{-1}	Net biological consumption rates of H^+ of colony

Supplementary Table 7. State variables. *Related to METHODS.*

Symbol	Unit	Definition
CH_2O	mol C (mol C)$^{-1}$	Carbohydrate
CS	mol C (mol C)$^{-1}$	Carbon skeleton
N	mol N (mol C)$^{-1}$	Fixed N
O_2	mol O_2 m^{-3}	Intracellular O_2
Fe_{PS}	μmol Fe (mol C)$^{-1}$	Fe in photosystems
Fe_{NF}	μmol Fe (mol C)$^{-1}$	Fe in active nitrogenase
Fe_{NF}^{NA}	μmol Fe (mol C)$^{-1}$	Fe in inactivated nitrogenase
Fe_{BF}	μmol Fe (mol C)$^{-1}$	Fe in buffer
O_2^M	mol O_2 m^{-3}	O_2 in microenvironment
CO_2^M	mol C m^{-3}	CO_2 in microenvironment
HCO_3^M	mol C m^{-3}	HCO_3^- in microenvironment
CO_3^M	mol C m^{-3}	CO_3^{2-} in microenvironment
H^M	mol H^+ m^{-3}	H^+ in microenvironment
OH^M	mol OH^- m^{-3}	OH^- in microenvironment

Note: The initial values (t = 0) of CH_2O, CS and N are set to be 0, and initial O_2 concentrations is the same as that of ambient O_2 (0.213 mol O_2 m^{-3}). Initial iron quotas are set the same as observational data from [18]. Initial components in the carbonate system are set as those under ambient or acidified conditions.

Supplementary Table 8. Comparison of modeled and observed growth rates under diurnally constant light intensity. *Related to METHODS.*

Growth rate (d^{-1})	Ambient (Fe′ = 40 pM)	Acidified (Fe′ = 40 pM)	Ambient (Fe′ = 1250 pM)	Acidified (Fe′ = 1250 pM)
Observation [a]	0.26 ± 0.02	0.19 ± 0.01	0.46 ± 0.01	0.37 ± 0.01
Model	0.25	0.18	0.46	0.36

[a] Data are from Shi, et al. [18].

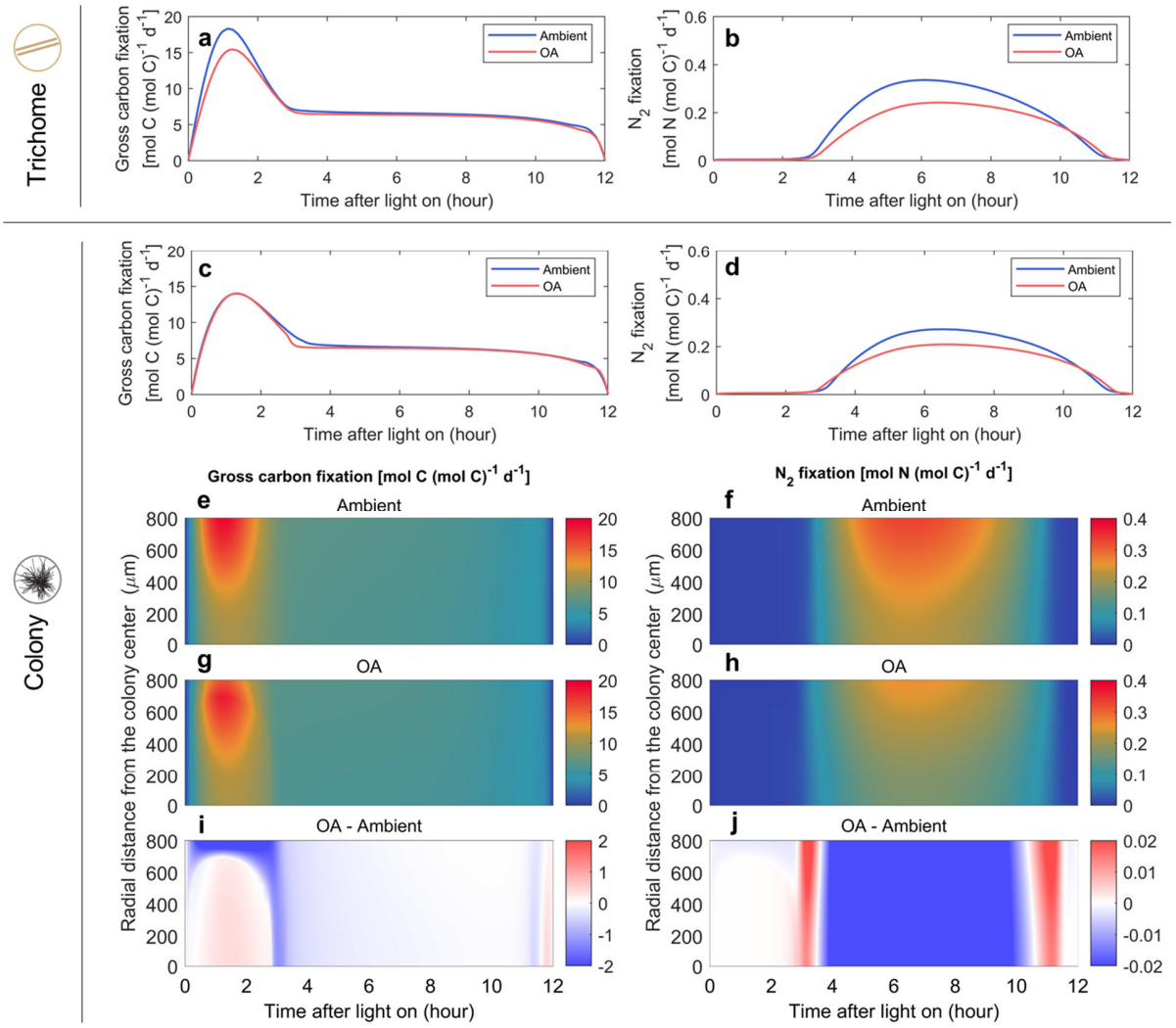

Supplementary Figure 1. Simulated results of *Trichodesmium* trichome and colony under replete Fe condition. *Related to Fig. 3.* (a, b) The comparison of the trichome model results under ambient and acidified (OA) conditions. The colony model results under ambient and OA conditions are compared in both (c, d) their average temporal and (e–j) spatiotemporal patterns. The spatiotemporal results include those under ambient conditions (e, f), OA conditions (g, h) and OA minus ambient results (i, j). Left panels present gross carbon fixation rates and right panels are N_2 fixation rates. The simulation was under a replete Fe′ concentration of 1250 pM. The figure of colony was modified from Klawonn, et al. [2].

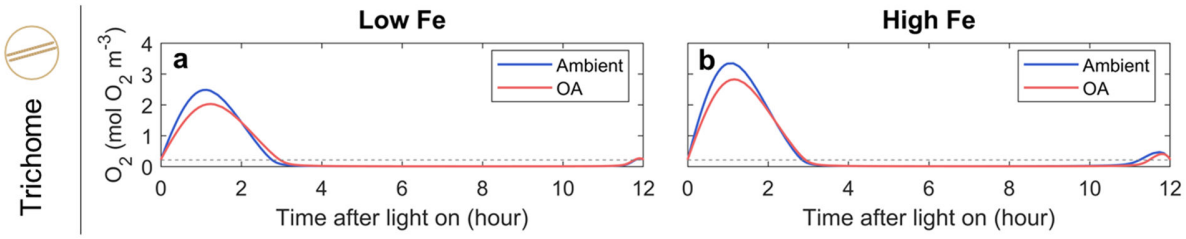

Supplementary Figure 2. Instantaneous intracellular oxygen concentrations of modeled *Trichodesmium* trichome during light period.

Related to Fig. 3. The trichome models were simulated under both ambient and acidified (OA) conditions with Fe′ at 40 and 1250 pM, respectively.

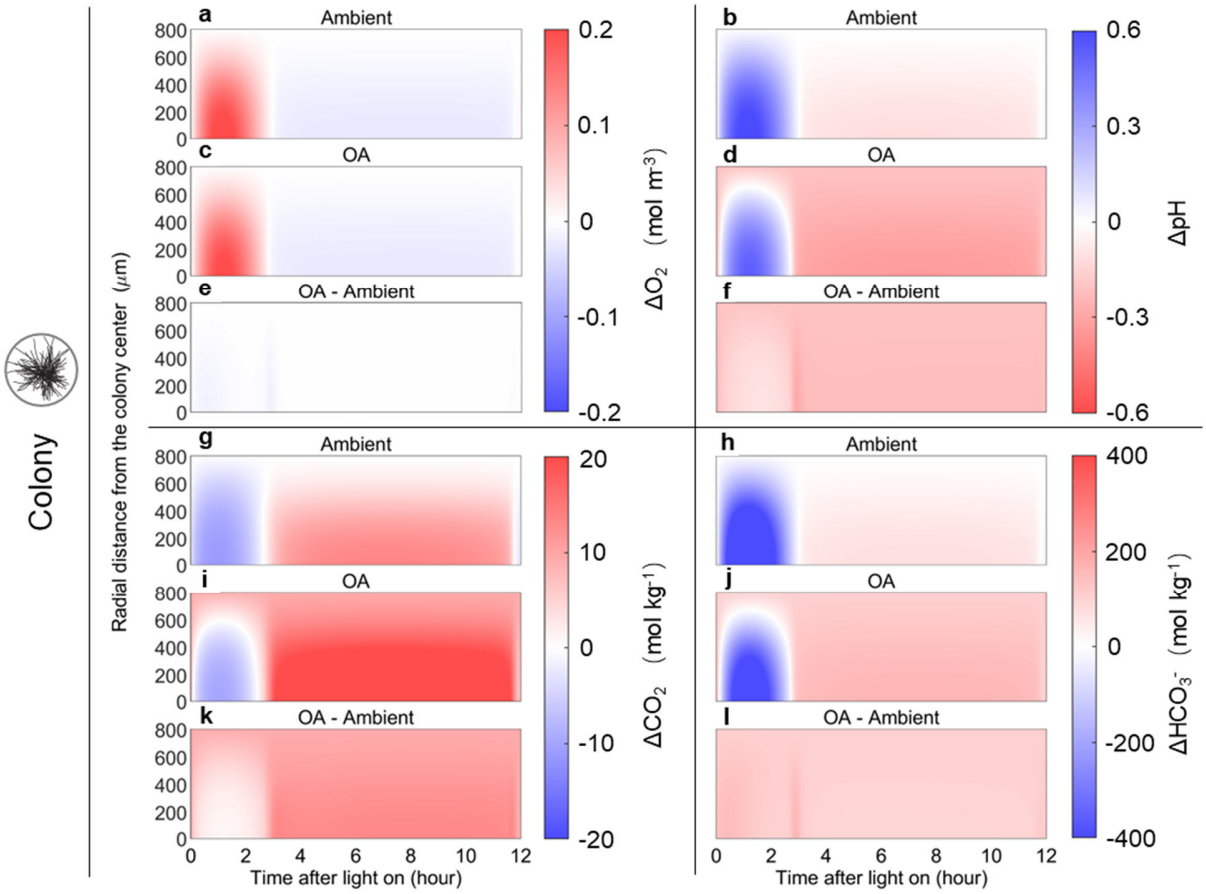

Supplementary Figure 3. Model experiments testing the impact of porosity gradients in biological processes on the formation of chemical gradients in the microenvironment of the colony under limiting Fe condition.

Related to Fig. 4. The colony models were simulated under both ambient (a, b, g, h) and OA (c, d, i, j) conditions with Fe′ at 40 pM. The concentrations of these parameters are shown as anomaly to those under ambient far-field conditions. The changes of these concentrations caused by OA are also displayed (e, f, k, l). The physical diffusion in the microenvironment was simulated using full porosity (constantly 1.0 from the center to the edge). The biological processes were simulated differently using the porosity with a gradient increasing to 1.0 at the outer edge of the colony based on Klawonn, et al. [2].

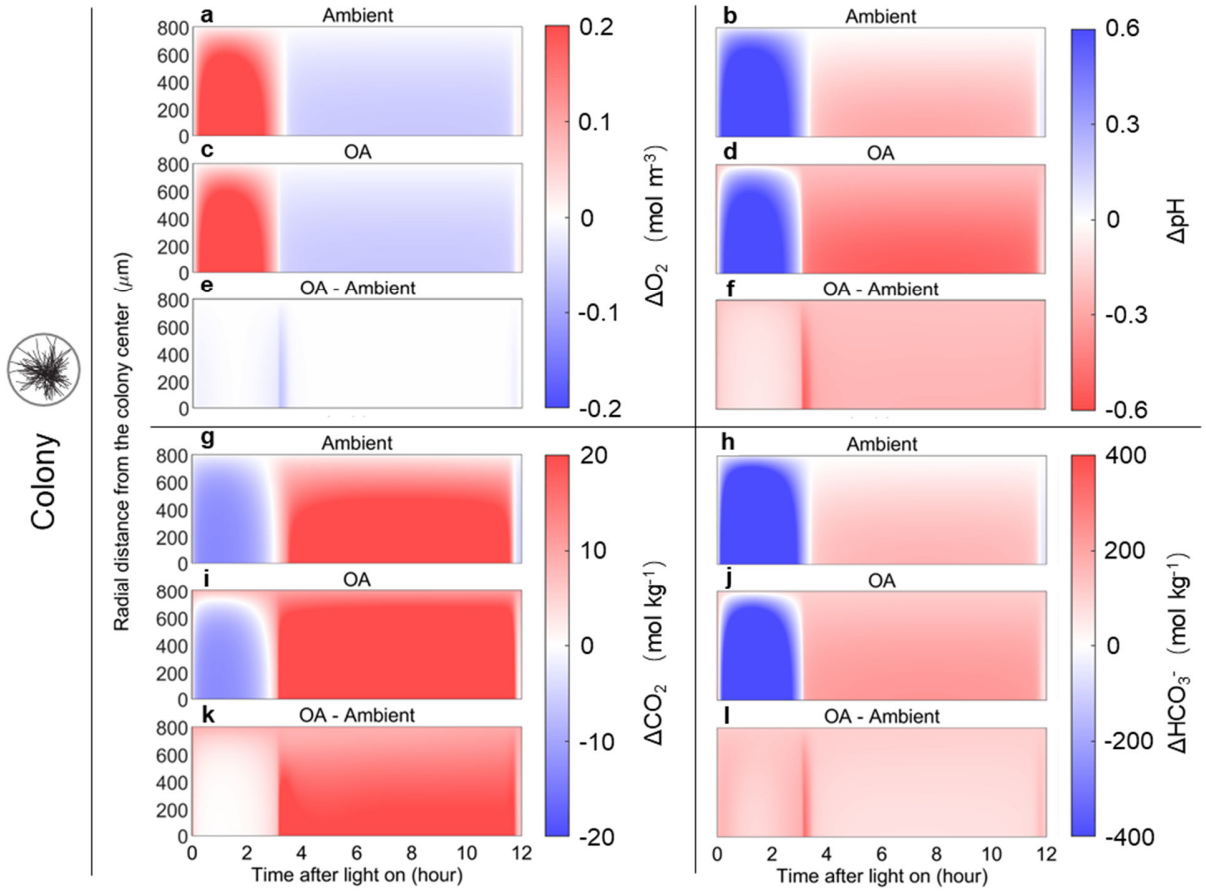

Supplementary Figure 4. Model experiments testing the impact of constant porosity on the formation of chemical gradients in the microenvironment of the colony under limiting Fe condition.

Related to Fig. 4. The colony models were simulated under both ambient (a, b, g, h) and OA (c, d, i, j) conditions with Fe′ at 40 pM. The concentrations of these parameters are shown as anomaly to those under ambient far-field conditions. The changes of these concentrations caused by OA are also displayed (e, f, k, l). Both physical diffusion and biological processes in the microenvironment were simulated using constant porosity (0.9937) from the center to the edge of the colony based on the average level of Klawonn, et al. [2]. Results show that the chemical gradients were formed even though the porosity was set constant, indicating the formation of chemical gradients was primarily attributed to diffusion limitation rather than high cell density in the center of the colony.

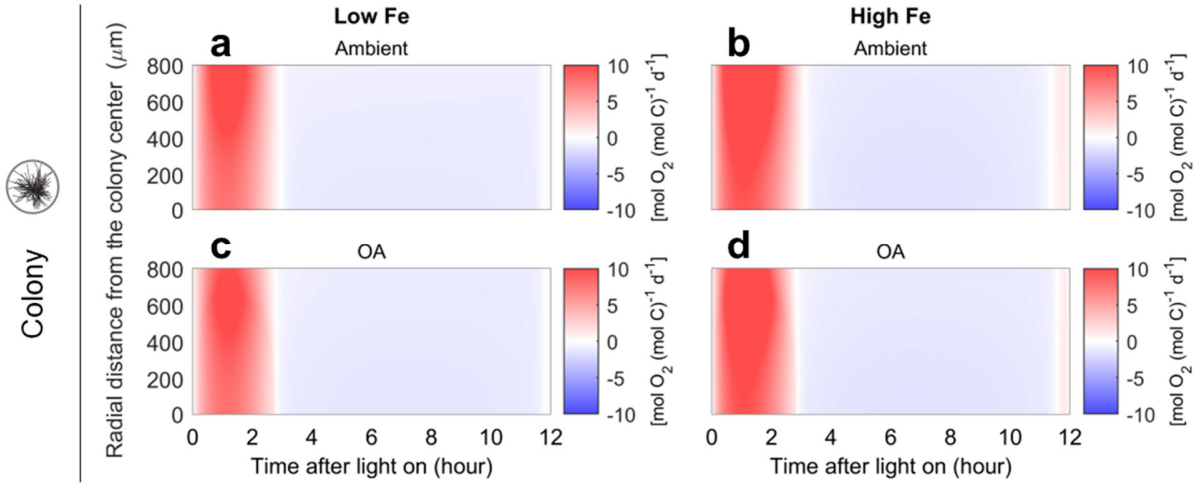

Supplementary Figure 5. Net O_2 production in the colony.

Related to Fig. 4. The colony models were simulated under ambient and acidified (OA) conditions and under low-Fe (Fe′ = 40 pM) and high-Fe (Fe′ = 1250 pM) conditions.

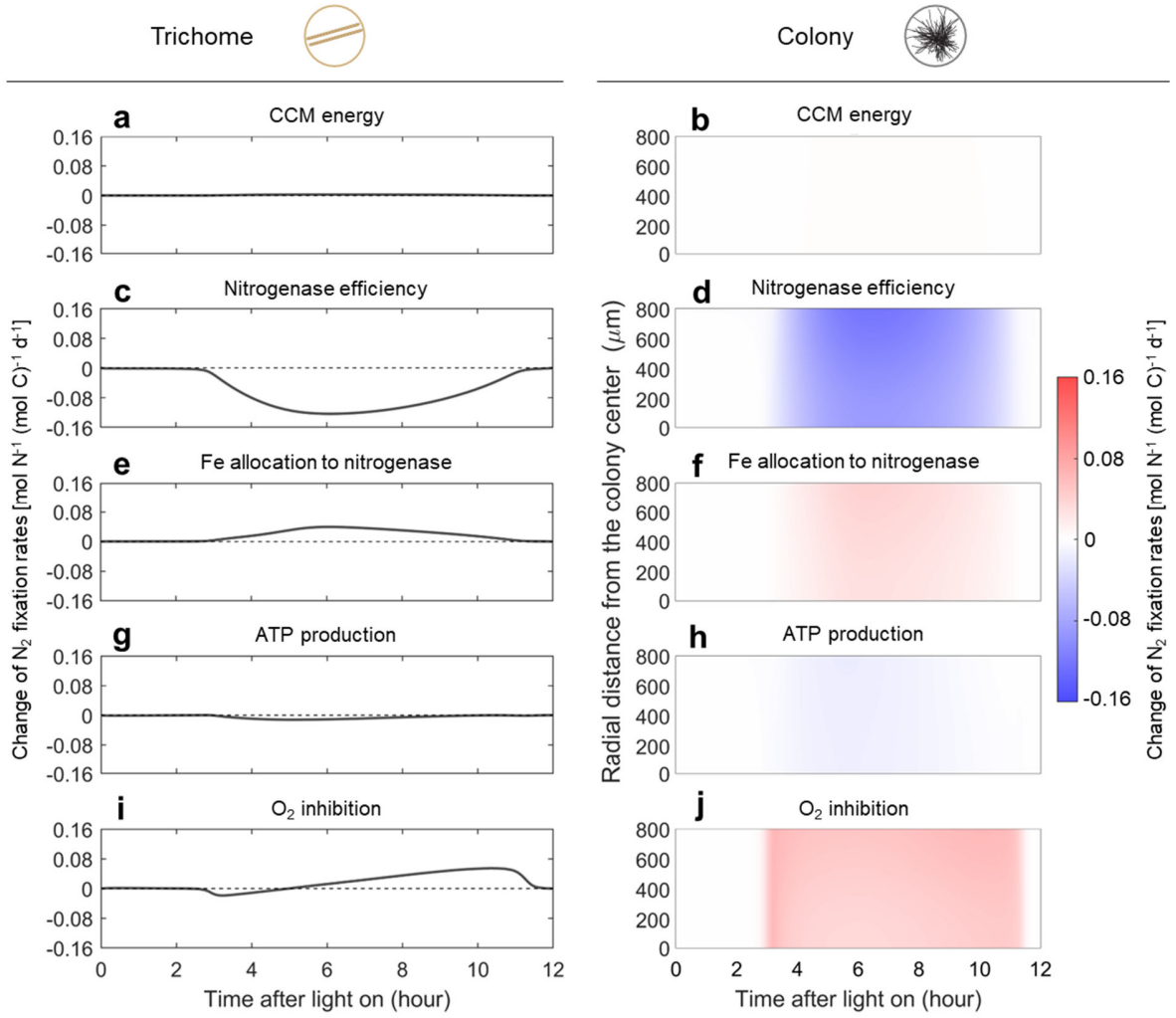

Supplementary Figure 6. Changes of N_2 fixation rates caused by each of OA effects under replete Fe conditions. *Related to Fig. 5.* The trichome (left column) and colony (right column) models were simulated under ambient or acidified (OA) conditions with Fe repletion (Fe′ = 1250 pM). Each OA effect is calculated as the absolute changes in N_2 fixation under OA conditions compared to ambient conditions, with only that specific effect implemented in the model. The shown OA effects include those on (a, b) energy savings by CCM, (c, d) the effect of pH on nitrogenase efficiency, (e, f) allocation of Fe to active nitrogenase, (g, h) inhibition on ATP production, and (i, j) the inhibition of N_2 fixation from intracellular O_2.

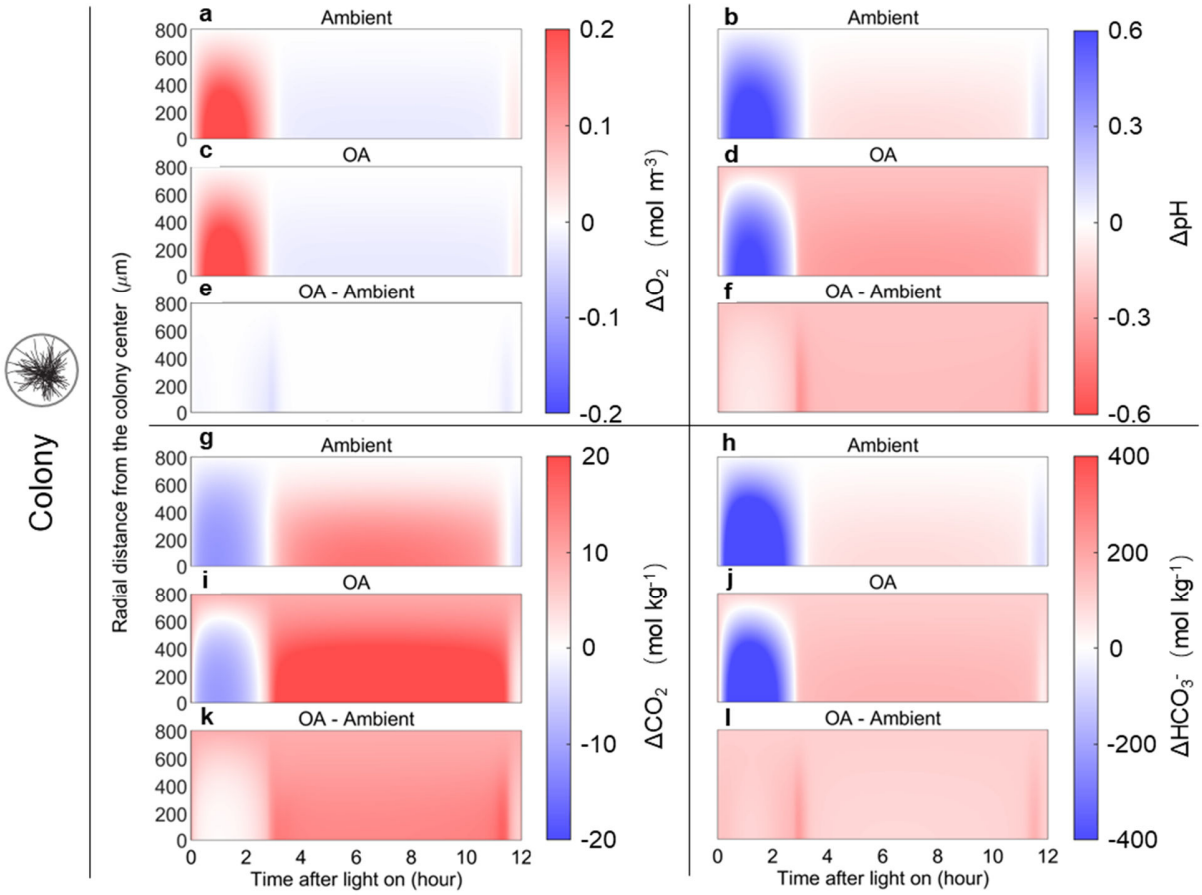

Supplementary Figure 7. Simulated O_2, pH, CO_2 and HCO_3^- concentrations in the microenvironment of the colony under replete Fe condition.

Related to Fig. 4. The colony models were simulated under both ambient (a, b, g, h) and OA (c, d, i, j) conditions with Fe′ at 1250 pM. The concentrations of these parameters are shown as anomaly to those under ambient far-field conditions. The changes of these concentrations caused by OA are also displayed (e, f, k, l).

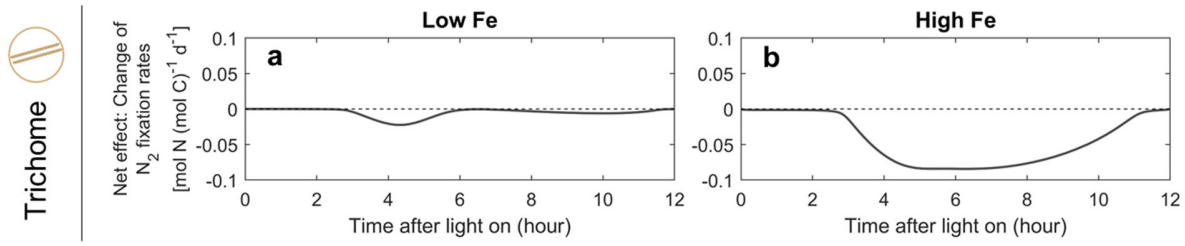

Supplementary Figure 8. Changes of N_2 fixation rates in *Trichodesmium* trichome caused by net effects between allocation of Fe to active nitrogenase and pH on nitrogenase efficiency.

Related to Fig. 5. The trichome models were simulated under both ambient and acidified (OA) conditions with Fe′ at 40 and 1250 pM, respectively.

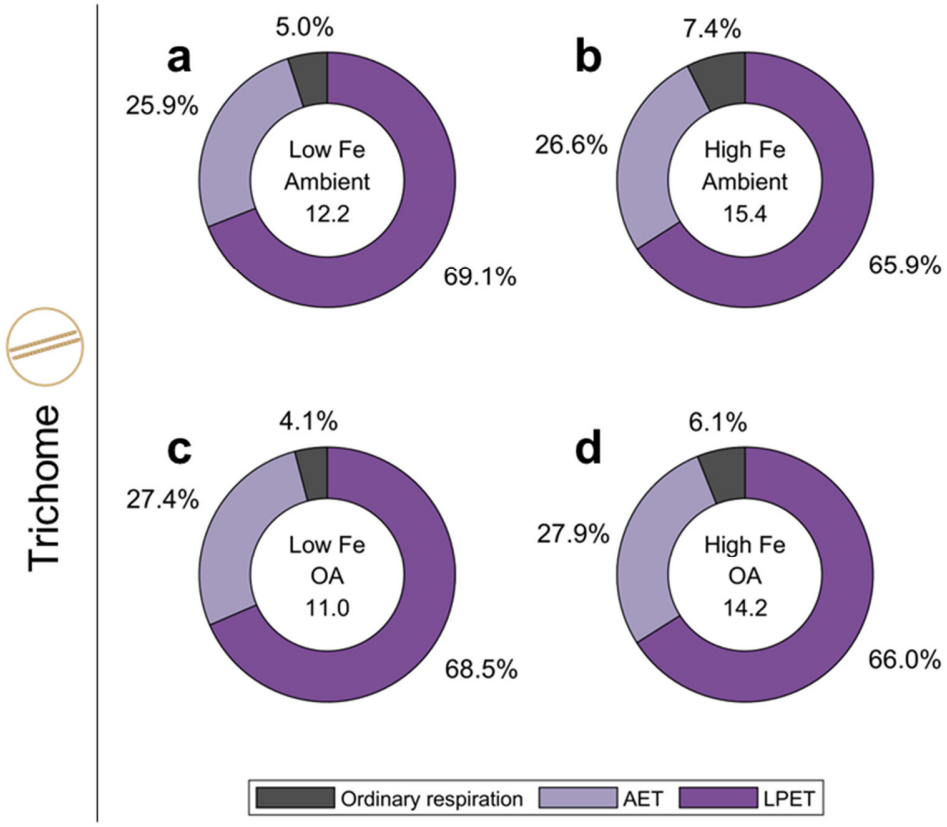

Supplementary Figure 9. Modeled daily-integrated energy (ATP) production of *Trichodesmium* trichome. *Related to DISCUSSION.* The trichome model was simulated under ambient (a, b) or acidified (OA) (c, d) conditions with Fe′ at 40 pM (a, c) or 1250 pM (b, d). The number in the inner circle represents the daily-integrated gross energy production rate [mol ATP (mol C)$^{-1}$ d^{-1}].

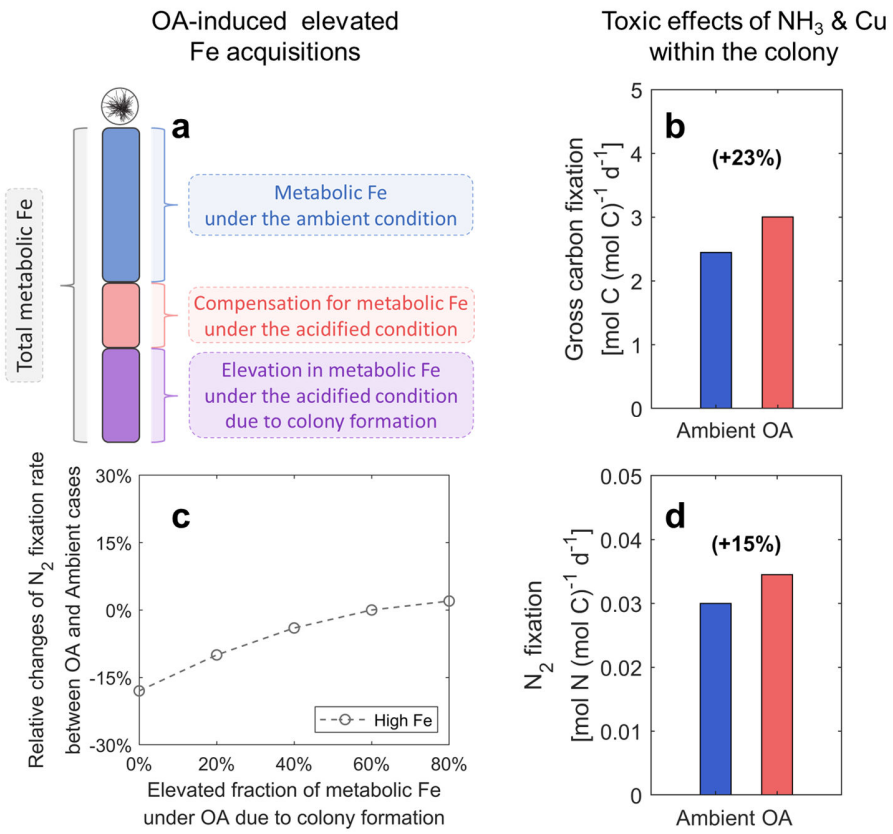

114

115 **Supplementary Figure 10.** Results of model experiments of other potential mechanisms of the OA effects on

116 *Trichodesmium* colonies under Fe repletion.

117 *Related to Fig. 6.* (a, c) OA-induced elevated Fe acquisition when *Trichodesmium* forms colonies: (a) Schematic

118 diagrams are for the metabolic Fe in modeled *Trichodesmium* colony. (c) Also shown are the relative changes of N_2

119 fixation rates in the modeled colony from acidified to ambient conditions.

120 (b, d) Toxic effects of ammonia and copper. The microenvironmental NH_4^+ concentration gradients decreases from

121 1.0 μmol L^{-1} in the center to 0.4 μmol L^{-1} at the edge. The colony models were simulated under ambient or acidified

122 (OA) conditions at a replete Fe′ level (1250 pM).

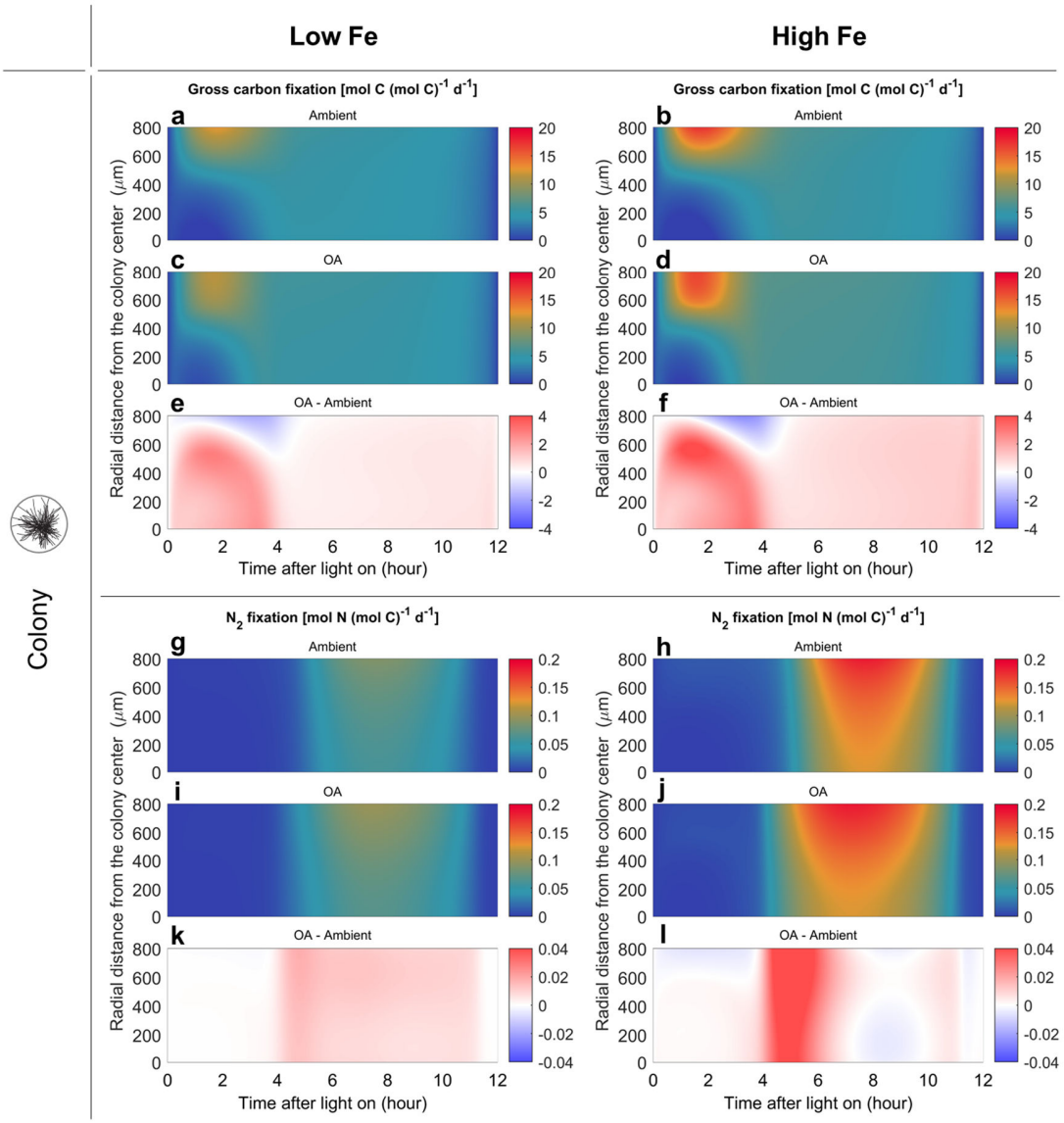

123

124 **Supplementary Figure 11.** Model results of *Trichodesmium* colony with toxicity effects of ammonia and copper.

125 *Related to Fig. 6 and DISCUSSION.* The colony models were simulated under ambient or acidified (OA) conditions.

126 Top panels present gross carbon fixation rate and bottom panels are N_2 fixation rates. The simulations were under

127 limiting Fe′ concentration of 40 pM (left column) or replete Fe′ of 1250 pM (right column). In the colony model,

128 microenvironmental NH_4^+ concentration profile was predefined according to the findings of Klawonn, et al. [2]. The

129 pattern of microenvironmental Cu was set the same as that of NH_4^+, with the highest concentration (1 nmol L^{-1}) at the

130 center of the colony. Red area (e, f, k, l) represents higher carbon or N_2 fixation rates under OA.

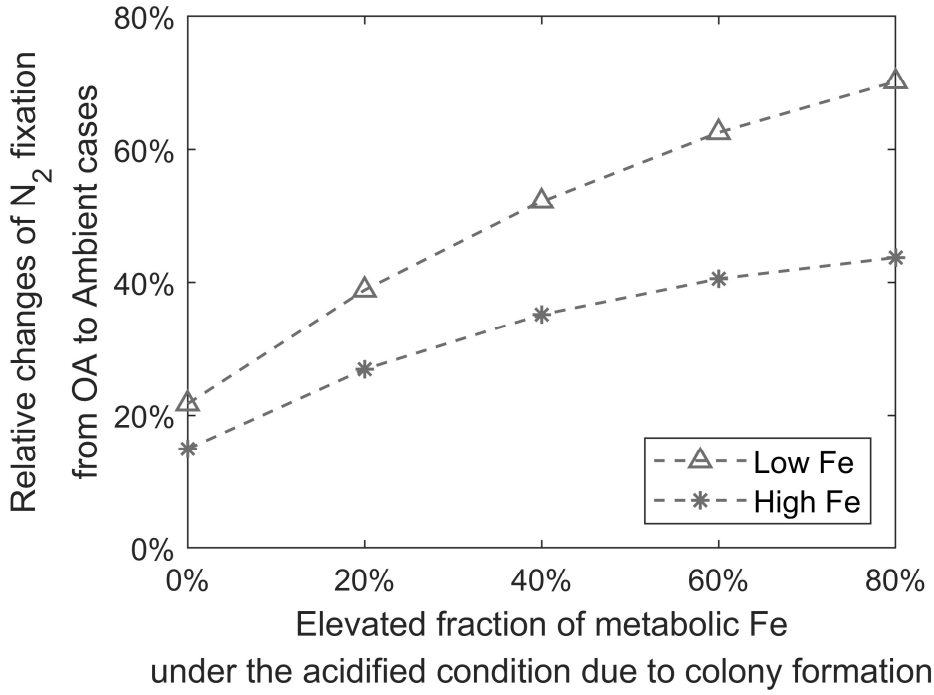

131

132 **Supplementary Figure 12.** Results of model experiments testing effects of elevated Fe acquisition in *Trichodesmium*

133 colonies when considering ammonia and copper toxicity.

134 *Related to Fig. 6 and DISCUSSION.* The colony models were simulated under ambient or acidified (OA) conditions

135 at limiting (40 pM) and replete (1250 pM) Fe′ level.

136

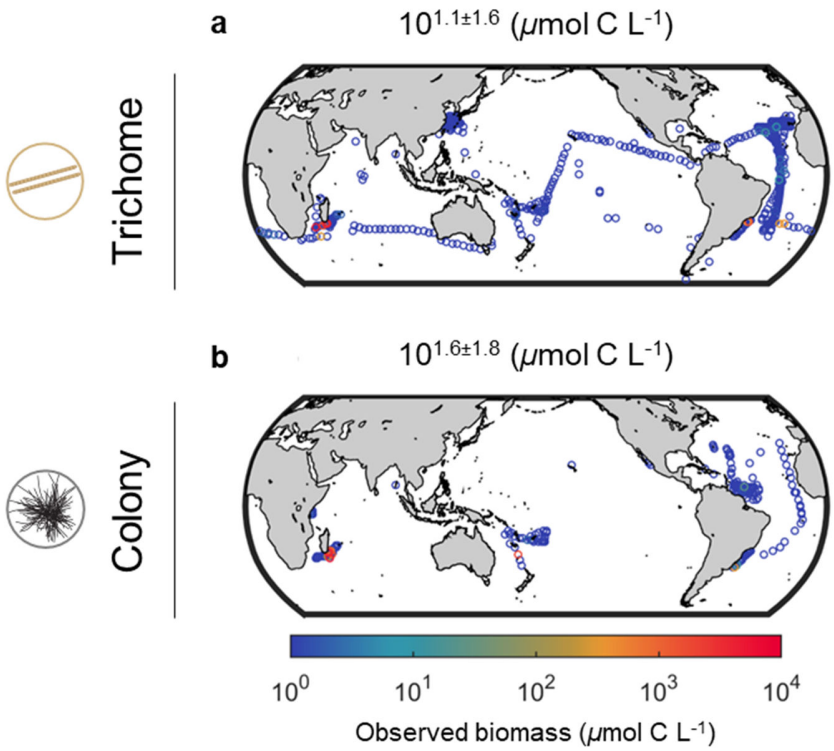

Supplementary Figure 13. The observed biomass of trichome and colony.

Related to Fig. 7 and DISCUSSION.

(a, b) Observations [19] with geometric mean and standard deviation. Values (b) represent colony biomass calculated from raw database data [19] with a 0.25 multiplier applied to adjust for seasonal occurrence of colonies [20].

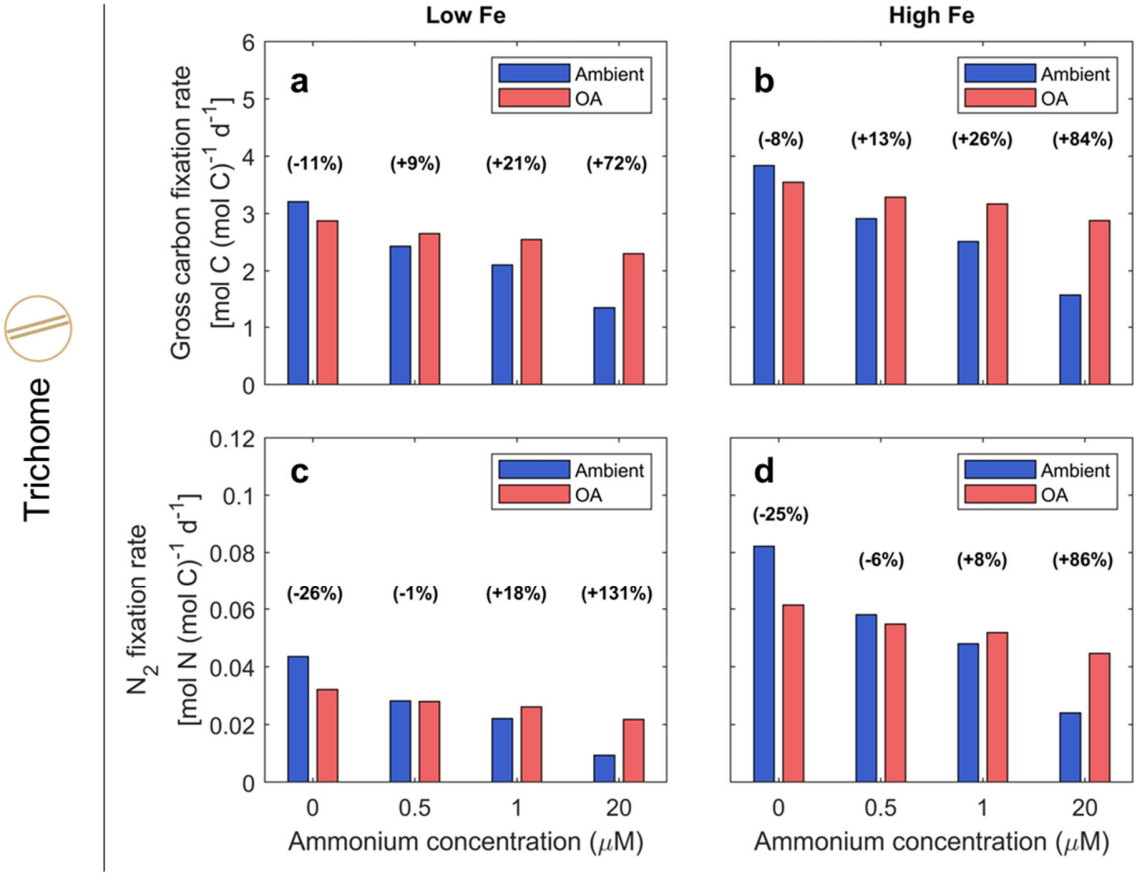

Supplementary Figure 14. Results of model experiments of toxic effects of ammonia and copper in free trichomes. *Related to DISCUSSION and METHODS.* The trichome models were simulated under ambient or acidified (OA) conditions and under limiting-Fe (Fe′ = 40 pM) and replete-Fe (Fe′ = 1250 pM) conditions. The concentration of total dissolved copper was set 1 nmol L^{-1}, which is at the same level as that of the YBC-II medium [21]. Model results were constrained using observations with artificially introduced toxicity [22,23].

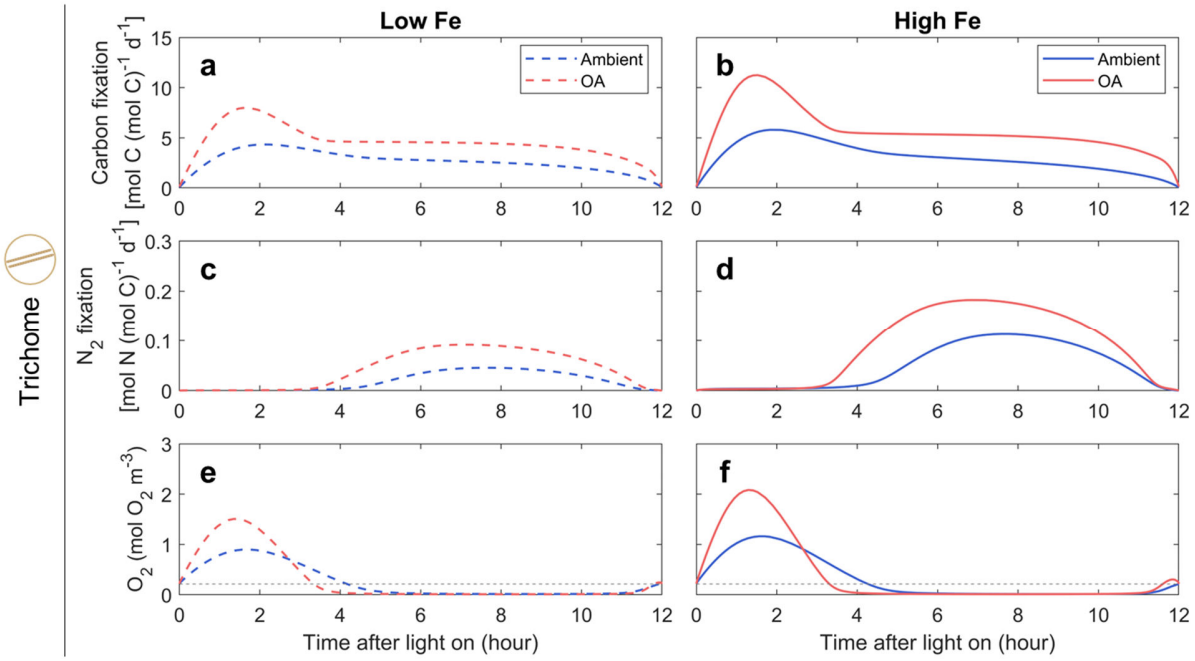

Supplementary Figure 15. Results of model experiments on OA effects when considering ammonia and copper toxicity in free trichomes.

Related to DISCUSSION and *METHODS.* The trichome models were simulated under ambient (blue lines) or acidified (OA) (red lines) conditions with Fe′ at 40 pM (a, c, e) or 1250 pM (b, d, f). The shown results include instantaneous rates of gross carbon fixation (a, b) and N_2 fixation (c, d), as well as intracellular O_2 concentrations (e, f). For the experiments, the concentration of total dissolved copper was set 1 nmol L^{-1}, which is at the same level as that of YBC-II medium [21]; the ammonium concentration was set at 20 μmol L^{-1} as Hong, et al. [22]. The black dashed lines in (e) and (f) represent the far-field extracellular O_2 concentration. In the presence of Cu and NH_3 toxicity, OA not only enhanced N_2 fixation potential of *Trichodesmium* free trichomes but also increased their carbon fixation rates. This led to greater carbohydrate accumulation during the early light period, which facilitated the formation of the low-O_2 window, further promoting N_2 fixation rates.

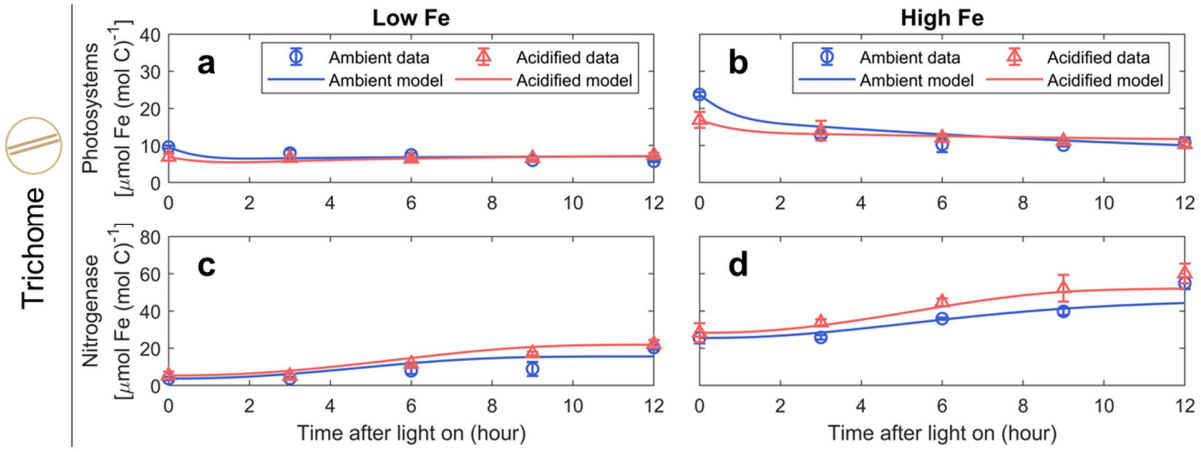

Supplementary Figure 16. Modeled and observed diurnal variations of Fe in photosystems and nitrogenase in *Trichodesmium* free trichome.

Related to METHODS. The observational data are from Shi, et al. [18]. The model was simulated under both ambient (blue lines) and acidified (red lines) conditions with a constant light intensity and Fe′ concentrations of 40 pM (a, c) and 1250 pM (b, d).

Supplementary Methods. Full model description. *Related to METHODS.*

We introduce the schemes of single trichome first, and then describe the model parametrizations of *Trichodesmium* colony.

1. Light intensity and photosynthetic pathways

The daytime light intensity (I, μmol m^{-2} s^{-1}) is [24]:

$$I(t) = I_{max} \cdot \sin(\frac{\pi \cdot t}{43{,}200}), \quad \text{(S1)}$$

where I_{max} is the maximal light intensity and t is the time (s) during a 12-hour light period.

Linear photosynthetic electron transfer (LPET) and alternative electron transfer (AET) are simulated in our model (Fig. 1a). Because (Mehler reaction)-mediated AET is probably the dominant AET in *Trichodesmium* [25], other AET (e.g., the cyclic electron transfer around photosystem I, the AET mediated by midstream oxidase with photosystem II, and the AET from photosystem II to the respiratory terminal oxidase respiratory terminal oxidase) [26], are not considered.

Both LPET and AET generate a proton gradient of 12 H^+ per 8 photons [9]. By assuming that 3 ATP are produced by the thylakoid ATP synthase with a proton gradient of 14 H^+, for 4 electrons through PET, LPET produces 2.6 ATP, with 2 NADPH and 1 O_2, while AET only produces 2.6 ATP [8,9,26].

The total PET rate [V_{PET}, mol electron (mol C)$^{-1}$ s^{-1}] is modulated by light intensity (I) and increases with the amount of Fe allocated to photosystems [Fe_{PS}, μmol Fe (mol C)$^{-1}$], and V_{PET} is inhibited by respiratory protection (RP) [V_{RP}, mol C (mol C)$^{-1}$ s^{-1}, described later] [27].

$$V_{PET} = v_{PET}^{max} \cdot \frac{Fe_{PS}}{Fe_{PS} + k_{Fe}^{PS}} \cdot (1 - e^{-\alpha_I \cdot I}) \cdot e^{-\beta \cdot V_{RP}}, \quad \text{(S2)}$$

where v_{PET}^{max} [mol electron (mol C)$^{-1}$ s^{-1}] is the maximal rate of PET, k_{Fe}^{PS} [μmol Fe (mol C)$^{-1}$] is the half-saturating coefficient of Fe_{PS} for PET, α_I (μmol^{-1} m^2 s) is the initial slope of PET versus light curve, and β [mol C (mol C)$^{-1}$ s] represents the degree of the inhibition effect from RP on PET.

To calculate the rates of LPET and AET [V_{LPET} and V_{AET} , mol electron (mol C)$^{-1}$ s^{-1}], the fraction of photosynthetic electrons flowing into AET (f_{AET}, dimensionless) is introduced in our model, and f_{AET} is calculated in each time step to fulfill the intracellular immediate requirement of ATP and NADPH [4].

$$V_{LPET} = V_{PET} \cdot (1 - f_{AET}), \quad \text{(S3)}$$

$$V_{AET} = V_{PET} \cdot f_{AET}. \quad \text{(S4)}$$

The ATP production rate of PET [V_{ATP}, mol ATP (mol C)$^{-1}$ s^{-1}] is contributed by both LPET and AET, and it is downregulated under OA [22]:

$$V_{ATP} = (V_{LPET} \cdot q_{LPET}^{ATP} + V_{AET} \cdot q_{AET}^{ATP}) \cdot 10^{OA^{PET} \cdot (pH - pH_{bsl})}, \quad \text{(S5)}$$

where $q_{LPET}^{ATP} = q_{AET}^{ATP} = 0.65$ mol ATP (mol electron)$^{-1}$are ratios of ATP to electron in LPET and AET [8,9,26], OA^{PET} (dimensionless) denotes the degree of OA impact on the ATP production by PET, pH (dimensionless) represents the extracellular pH value at the cell surface, and pH_{bsl} = 8.08 refers to the baseline pH value.

NADPH production by LPET is unlike ATP production, which is driven by the proton (H^+) gradient between the lumen and stroma [8,9]. Therefore, its rate is assumed to be not impacted by the reduction in the pH value under OA:

$$V_{NAPDH} = V_{LPET} \cdot q_{LPET}^{NADPH}, \quad \text{(S6)}$$

where $q_{LPET}^{NADPH} = 0.5$ mol NADPH (mol electron)$^{-1}$ is the ratio of NADPH to electron in LPET [8].

The O_2 production rate [V_{O_2}, mol O_2 (mol C)$^{-1}$ s^{-1}] is:

$$V_{O_2} = V_{LPET} \cdot q_{LPET}^{O_2}, \quad \text{(S7)}$$

where $q_{LPET}^{O_2} = 0.25$ mol O_2 (mol electron) $^{-1}$ is the ratio of O_2 to electron in LPET [8,9].

2. N_2 fixation

N_2 fixation requires both ATP and NADPH [10,11]. The maximal N_2 fixation rate [V_{NF}^{max}, mol N (mol C)$^{-1}$ s^{-1}] is calculated based on the assumption that produced ATP and NADPH of PET completely sustain N_2 fixation.

$$V_{NF}^{max} = \frac{V_{ATP}}{q_{NF}^{ATP}}, \quad \text{(S8)}$$

where q_{NF}^{ATP} = 9 mol ATP (mol N)$^{-1}$ is ATP:N ratio in N_2 fixation [10,11].

The N_2 fixation rate [V_{NF}, mol N (mol C)$^{-1}$ s^{-1}] is also regulated by the Fe quota in nitrogenase [Fe_{NF}, μmol Fe (mol C)$^{-1}$] and inhibited by intracellular O_2 [O_2, mol O_2 m^{-3}] [28]. Under OA, the reduced pH value (i.e., increased H^+ concentration) lowers the efficiency of nitrogenase [1,22] while the energy saved from CCM can benefit N_2 fixation [29].

$$V_{NF} = V_{NF}^{max} \cdot \frac{Fe_{NF}}{Fe_{NF} + k_{Fe}^{NF}} \cdot 10^{pH - pH_{bsl}} \cdot (1 - \frac{O_2}{O_2 + k_{O_2}^{NF}}) + V_{NF}^{CCM}, \quad \text{(S9)}$$

where k_{Fe}^{NF} [μmol Fe (mol C)$^{-1}$] and $k_{O_2}^{NF}$ (mol O_2 m^{-3}) are half-saturating coefficients of Fe_{NF} and O_2 for N_2 fixation, V_{NF}^{CCM} [mol N (mol C)$^{-1}$ s^{-1}] represents the elevated N_2 fixation rate driven by CCM energy saving [$V_{ATP}^{CCM,\ saving}$, mol ATP (mol C)$^{-1}$ s^{-1}] under OA.

$$V_{NF}^{CCM} = \frac{V_{ATP}^{CCM,\ saving}}{q_{NF}^{ATP}} \cdot \frac{Fe_{NF}}{Fe_{NF} + k_{Fe}^{NF}} \cdot 10^{pH - pH_{bsl}} \cdot (1 - \frac{O_2}{O_2 + k_{O_2}^{NF}}). \quad \text{(S10)}$$

<u>3. CO_2 concentrating mechanism</u>

The energy consumption rate for CCM [V_{ATP}^{CCM}, mol ATP (mol C)$^{-1}$ s^{-1}] is calculated based on the requirement of HCO_3^- for carbon fixation [V_{CF}, mol C (mol C)$^{-1}$ s^{-1}] and the cost for per HCO_3^- transportation [$q_{HCO_3^-}^{ATP}$ = 0.5 mol ATP (mol C)$^{-1}$] [1,13,30].

$$V_{ATP}^{CCM} = (V_{CF} - f_{RP}^{CF} \cdot V_{RP} - \frac{T_{CO_2}}{Q_C}) \cdot q_{CCM}^{ATP}, \quad \text{(S11)}$$

where V_{RP} [mol C (mol C)$^{-1}$ s^{-1}] is the respiratory protection rate, f_{RP}^{CF} represents the fraction of produced CO_2 by respiratory protection to support carbon fixation, T_{CO_2} (mol CO_2 m^{-3} s^{-1}) is the diffusion rate of CO_2 between cytoplasm and extracellular environment, Q_C = 18333 mol C m^{-3} is the cellular carbon biomass quota [15].

The elevation of CO_2 concentration (CO_2, mol C m^{-3}) as seawater acidifies can lower the energy need for CCM by reducing the requirement for HCO_3^- [29,31-33]:

$$V_{ATP}^{CCM,\ saving} = (\frac{T_{CO_2}}{Q_C} - \frac{T_{CO_2}^{bsl}}{Q_C}) \cdot q_{CCM}^{ATP} \quad \text{(S12)}$$

where $T_{CO_2}^{bsl}$ (mol CO_2 m^{-3} s^{-1}) is the diffusion rate of CO_2 between cytoplasm and extracellular environment under baseline condition.

4. Carbon fixation

Carbon fixation also requires both NADPH and ATP [12], and consumption rates [V_{NADPH}^{CF} and V_{ATP}^{CF}, mol NADPH (mol C)$^{-1}$ s^{-1} and mol ATP (mol C)$^{-1}$ s^{-1}] are:

$$V_{NADPH}^{CF} = V_{CF} \cdot q_{CF}^{NADPH}, \tag{S13}$$

$$V_{ATP}^{CF} = V_{CF} \cdot q_{CF}^{ATP}. \tag{S14}$$

V_{CF} is solved at each time step with f_{AET}, based on the consumption that total NADPH and ATP production by PET are immediately and fully utilized by intracellular process:

$$V_{NADPH} = V_{NADPH}^{CF} + V_{NADPH}^{NF}, \tag{S15}$$

$$V_{ATP} = (V_{ATP}^{CCM} + V_{ATP}^{CF} + V_{ATP}^{NF}) \cdot (1 + \gamma_{MT}), \tag{S16}$$

where γ_{MT} (dimensionless) represents the ratio of ATP consumption by maintenance to other processes [1].

The carbon skeleton production rate [V_{CS}, mol C (mol C)$^{-1}$ s^{-1}] is stimulated by carbohydrate [CH_2O, mol C (mol C)$^{-1}$] and downregulated by its own accumulation [CS, mol C (mol C)$^{-1}$]:

$$V_{CS} = v_{CS}^{max} \cdot \frac{CH_2O}{CH_2O + k_{CH_2O}^{CS}} \cdot \frac{CS_{max} - CS}{CS_{max}}, \tag{S17}$$

where v_{CS}^{max} [mol C (mol C)$^{-1}$ s^{-1}] is the maximal production rate of the carbon skeleton, $k_{CH_2O}^{CS}$ [mol C (mol C)$^{-1}$] is the half-saturation constant of carbohydrates for carbon skeleton production, and CS_{max} [mol C (mol C)$^{-1}$] is the maximum CS storage.

5. Respiratory protection

Respiratory protection rate is regulated by the requirement of N_2 fixation and intracellular O_2 [4,5,34]:

$$V_{RP} = v_{RP}^{max} \cdot (1 - e^{-\alpha_I \cdot I}) \cdot \frac{CS}{CS + k_{CS}} \cdot \left(\frac{N_{max} - N}{N_{max}}\right) \cdot \frac{O_2}{O_2 + k_{O_2}^{NF}}, \tag{S18}$$

where v_{RP}^{max} [mol C (mol C)$^{-1}$ s^{-1}] is the maximal respiratory protection rate, k_{CS} [mol C (mol C)$^{-1}$] is the half-saturating coefficient of the carbon skeleton for respiratory protection, and N_{max} [mol N (mol C)$^{-1}$] is the maximal N storage.

The O_2 consumption by RP [$V_{O_2}^{RP}$, mol O_2 (mol C)$^{-1}$ s^{-1}] is:

$$V_{O_2}^{RP} = V_{RP} \cdot q_C^{O_2}, \tag{S19}$$

where $q_C^{O_2}$ [mol O_2 (mol C)$^{-1}$] is the ratio of O_2 to carbon in carbohydrate respiration.

6. O_2 and CO_2 diffusion

The rate of O_2 diffusion (T_{O_2}, mol O_2 m^{-3} s^{-1}) between the intracellular cytoplasm and the extracellular environment is parameterized by adopting the scheme in Staal, et al. [35]:

$$T_{O_2} = \frac{-2 \cdot \pi \cdot d_{O_2} \cdot L}{V} \cdot \left\{ \frac{1}{\varepsilon} \cdot \ln\left(\frac{R}{R + L_g}\right) - \ln\left(\frac{R + L_g + L_b}{R + L_g}\right) \right\}^{-1} \cdot (O_2^E - O_2), \tag{S20}$$

where d_{O_2} (m^2 s^{-1}) is the O_2 diffusion coefficient in seawater, ε (dimensionless) is the ratio of the O_2 diffusion coefficient of the cell membrane relative to d_{O_2}, L (m) and V (m^3) are the length and the volume of the trichome, R (m) is the radius of the cytoplasm, L_g (m) is the thickness of the cell membrane, L_b (m) is the thickness of the boundary layer, O_2^E is the extracellular far-field O_2 concentration.

The CO_2 diffusion rate between cytoplasm and extracellular environment is

$$T_{CO_2} = \frac{-2 \cdot \pi \cdot d_{CO_2} \cdot L}{V} \cdot \left\{ \frac{1}{\varepsilon_{CO_2}} \cdot \ln\left(\frac{R}{R + L_g}\right) - \ln\left(\frac{R + L_g + L_b}{R + L_g}\right) \right\}^{-1} \cdot CO_2^E, \tag{S21}$$

where d_{CO_2} (m^2 s^{-1}) is the CO_2 diffusion coefficient in seawater, ε_{CO_2} (dimensionless) is the ratio of the CO_2 diffusion coefficient of the cell membrane relative to d_{CO_2}, CO_2^E is the extracellular far-field CO_2 concentration. CO_2 concentration in the cytoplasm was not simulated but set 0 based on the assumption that CO_2 in the cytoplasm was assumed to be quickly transferred into carboxysome or leak into extracellular environment.

$T_{CO_2}^{bsl}$ is calculated based on the extracellular far-field CO_2 concentration under baseline condition:

$$T_{CO_2}^{bsl} = \frac{-2 \cdot \pi \cdot d_{CO_2} \cdot L}{V} \cdot \left\{ \frac{1}{\varepsilon_{CO_2}} \cdot \ln\left(\frac{R}{R + L_g}\right) - \ln\left(\frac{R + L_g + L_b}{R + L_g}\right) \right\}^{-1} \cdot CO_{2,\,bsl}^E. \tag{S22}$$

7. Intracellular Fe pools and translocation

Trichodesmium can uptake more Fe than that required by its metabolism (called "luxury uptake") particularly under high-Fe conditions, and the excess Fe is stored to enable the survival in low-iron environments [36,37]. Therefore, the total intracellular Fe quota [Fe, μmol Fe (mol C)$^{-1}$] consists of Fe in metabolism and storage [Fe_M and Fe_{ST}, μmol Fe (mol C)$^{-1}$], calculated based on the threshold level of Fe [Fe_{TH}, μmol Fe (mol C)$^{-1}$] [1]:

$$Fe_{TH} = Fe_{TH}^{bsl} \cdot [1 + OA^{ST} \cdot (10^{pH_{bsl} - pH} - 1)], \quad \text{(S23)}$$

$$Fe_M = Fe, \quad \text{when } Fe \le Fe_{TH}, \quad \text{(S24)}$$

$$Fe_M = Fe_{TH} + (1 - f_{ST}) \cdot (Fe - Fe_{TH}), \text{ when } Fe > Fe_{TH}, \quad \text{(S25)}$$

where Fe_{TH}^{bsl} [μmol Fe (mol C)$^{-1}$] is the threshold level of Fe under the baseline condition, OA^{ST} (dimensionless) is the coefficient representing the strength of OA impact on Fe_{TH}, f_{ST} (dimensionless) is the fraction of luxury Fe uptake.

Fe allocations are among Fe_M, including Fe in photosystems, active nitrogenase, inactivated nitrogenase, maintenance and buffer [Fe_{PS}, Fe_{NF}, Fe_{NF}^{NA}, Fe_{MT} and Fe_{BF}, μmol Fe (mol C)$^{-1}$]. Fe in maintenance is set diurnally constant at 10% of Fe_M under ambient and acidified conditions [1]. Fe used in the photosystems and nitrogenase is from the buffer pool [34].

Ocean acidification seemingly does not affect the general diurnal patterns of both Fe_{PS} and Fe_{NF} but their initial levels at the beginning of the light period [18], predefined in our model using observations [18]. The differences in the absolute amount of Fe_{PS} or Fe_{NF} between ambient and acidified conditions [18] were represented in the optimized maximal Fe translocation rates of photosystems or nitrogenase (Supplementary Table 5), which ensured optimal intracellular Fe allocations to achieve the maximal growth rate [3].

The synthesis rate of photosystems [T_{PS}^{BF}, μmol Fe (mol C)$^{-1}$ s^{-1}] is stimulated by light intensity and gradually saturated with Fe_{PS}:

$$T_{PS}^{BF} = TF_{PS_{max}}^{BF} \cdot (1 - e^{-\alpha_i \cdot I}) \cdot (1 - \frac{Fe_{PS}}{Fe_{PS} + k_{Fe_{PS}}^{PS_{syn}}}), \quad \text{(S26)}$$

where $T_{PS_{max}}^{BF}$ [μmol Fe (mol C)$^{-1}$ s^{-1}] is the maximal synthesis rate of photosystems, $k_{Fe_{PS}}^{PS_{syn}}$ [μmol Fe (mol C)$^{-1}$] is the half-saturating coefficients of Fe_{PS} for the synthesis of photosystems.

The decomposition rate of photosystems [T_{BF}^{PS}, μmol Fe (mol C)$^{-1}$ s^{-1}] is stimulated by Fe_{PS} but inhibited by respiratory protection [27]:

$$T_{BF}^{PS} = T_{BF_{max}}^{PS} \cdot \frac{Fe_{PS}}{Fe_{PS} + k_{Fe_{PS}}^{PS_{dec}}} \cdot e^{-\beta \cdot V_{RP}}, \quad \text{(S27)}$$

where $T_{BF_{max}}^{PS}$ [μmol Fe (mol C)$^{-1}$ s^{-1}] is the maximal decomposition rate of photosystems, $k_{Fe_{PS}}^{PS_{dec}}$ [μmol Fe (mol C)$^{-1}$] is the half-saturating coefficient of Fe_{PS} for the decomposition of photosystems. Fe released from decomposed photosystems returns to buffer pool [34].

The nitrogenase synthesis rate [T_{NF}^{BF}, μmol Fe (mol C)$^{-1}$ s^{-1}] is:

$$\Phi = (1 - e^{-\alpha_i \cdot I}) \cdot \frac{CS}{CS + k_{CS}} \cdot (\frac{N_{max} - N}{N_{max}}), \quad \text{(S28)}$$

$$T_{NF}^{BF} = T_{NF_{max}}^{BF} \cdot \Phi \cdot \frac{Fe_{BF}}{Fe_{BF} + k_{Fe_{BF}}^{NF_{syn}}}, \quad \text{(S29)}$$

where Φ represents the intracellular requirement of N_2 fixation, $T_{NF_{max}}^{BF}$ [μmol Fe (mol C)$^{-1}$ s^{-1}] is the maximal nitrogenase synthesis rate, k_{CS} [mol C (mol C)$^{-1}$] and $k_{Fe_{BF}}^{NF_{syn}}$ [μmol Fe (mol C)$^{-1}$] are half-saturating coefficients of the carbon skeleton and Fe_{BF} for the synthesis of nitrogenase, respectively, N_{max} [mol N (mol C)$^{-1}$] is the maximal N storage. Note that the requirement of N_2 fixation (Φ) is assumed to be stimulated by the increase of light and the production of CS stimulates but be suppressed by the accumulation of fixed N lowers the requirement.

The decomposition of nitrogenase seems to occur at night [18,38], and therefore it is not considered during the light period in our model. Notably, nitrogenase is inhibited upon exposure to O_2, flowing into the pool of inactivated nitrogenase [27] at the rate [T_{NF}^{NA}, μmol Fe (mol C)$^{-1}$ s^{-1}]:

$$T_{NF}^{NA} = T_{NF_{max}}^{NA} \cdot \frac{Fe_{NF}}{Fe_{NF} + k_{Fe}^{NF}} \cdot \frac{O_2}{O_2 + k_{O_2}^{NF}}, \quad \text{(S30)}$$

where $T_{NF_{max}}^{NA}$ [μmol Fe (mol C)$^{-1}$ s^{-1}] is the maximal inactivation rate of nitrogenase.

Note that The Fe in nitrogenase and photosystems from Shi, et al. [18] were estimated from observed protein content, based on Fe atoms in per protein. PSII, Cyt *b6f*, PSI and Ferredoxin together represents photosystems. Cyt *b6f* and Ferredoxin were not measured in Shi, et al. [18] but estimated by assuming Cyt *b6f*:PSII = 1:1 in Fe quota and Ferredoxin:PSI = 1:1 in protein content. Further details are in the supplementary information in [1].

8. Integration of state variables during the daytime

The diurnal change rates (basically normalized to carbon biomass) of CH_2O, CS, N, intracellular O_2 and Fe are represented in ordinary differential equations (ODEs). Note that O_2 is in a unit volumetric concentration (mol O_2 m^{-3}):

$$\frac{dCH_2O}{dt} = V_{CF} - V_{CS} - V_{RP}, \quad \text{(S31)}$$

$$\frac{dCS}{dt} = V_{CS}, \quad \text{(S32)}$$

$$\frac{dN}{dt} = V_{NF}, \quad \text{(S33)}$$

$$\frac{dO_2}{dt} = (V_{O_2} - V_{O_2}^{RP}) \cdot Q_C + T_{O_2}, \quad \text{(S34)}$$

$$\frac{dFe_{PS}}{dt} = T_{PS}^{BF} - T_{BF}^{PS}, \quad \text{(S35)}$$

$$\frac{dFe_{NF}}{dt} = T_{NF}^{BF} - T_{NF}^{NA}, \quad \text{(S36)}$$

$$\frac{dFe_{NF}^{NA}}{dt} = T_{NF}^{NA}, \quad \text{(S37)}$$

$$\frac{dFe_{BF}}{dt} = T_{BF}^{PSI} - T_{PSI}^{BF} \cdot + T_{NF}^{BF}. \quad \text{(S38)}$$

ODEs are run over a 12-hour light period with ode15s integrator of MATLAB [39].

9. Biosynthesis and growth rate

Trichodesmium might store newly fixed C and N during the daytime and assimilate them into biomass mainly during the dark period [40]. Therefore, for simplification, no biomass synthesis occurs during the light period in the model. Instead, the model calculates the amount of biomass [*Bio*, mol C (mol C)$^{-1}$] that can be synthesized using the carbohydrates, carbon skeletons and fixed N at the end of the light period. *Bio* is the smaller value of N-based (Bio_N) and C-based biomass (Bio_C), with Bio_N calculated by dividing fixed N to the molar N:C (0.159) [17]. Bio_C is calculated from the carbohydrates and carbon skeleton considering mass and energy balance. Notably, like PET, the impact of OA on the energy production by respiration is considered.

The energy needed for biosynthesis is from the respiration of carbohydrates ($CH_2O_{BIO}^{RESP}$):

$$Bio_C \cdot q_{BIO}^{ATP} \cdot (1 + \gamma_{MT}) = CH_2O_{BIO}^{RESP} \cdot q_{RESP}^{ATP} \cdot 10^{OA^{RESP} \cdot (pH - pH_{bsl})}, \quad \text{(S39)}$$

where q_{BIO}^{ATP} = 2 mol ATP (mol C)$^{-1}$ is the ATP requirement rate by biosynthesis [5], and q_{RESP}^{ATP} = 5 mol ATP (mol C)$^{-1}$ is the ATP production rate from respiring carbohydrates [14], OA^{RESP} (dimensionless) represents the strength of OA impact on the ATP production by respiration at

night. Given that the respiratory electron transfer chain shares the apparatuses in the PET chain and its energy production is also driven by the proton gradient [41], OA^{RESP} is set the same as OA^{PET}.

Meanwhile, the non-respired carbohydrates and all the carbon skeletons are involved in biosynthesis:

$$Bio_C = CH_2O - CH_2O_{BIO}^{RESP} + CS. \quad \text{(S40)}$$

Bio_C then can be solved from the above two equations. Note that the carbohydrate respiration calculated in this step is counted in the daily integrated respiration as the ordinary respiration.

Noting that all the rates have been normalized to carbon biomass, *Bio* is therefore the relative increase in biomass over one day. The growth rate (G) is then the natural log of (1 + *Bio*) divided by 1 day.

10. Colony model framework

The colony is modeled as a porous sphere (the radius, R_C = 800 μm), exhibiting spatially variable porosity with the variable porosity [$\psi(r)$, dimensionless] from the center to the edge of colony [2]. The porosity [$\psi(r)$] is calculated as the ratio of the non-biological volume to the sum of non-biological and biological volumes at the location, from which to the center of colony the radical distance is r (m), using the scheme in Klawonn, et al. [2]:

$$\psi(r) = 1 - 1.7141 \times 10^{-3} \cdot [1 + \tanh(2 - (2r/R_C - 0.6)/0.3]. \quad \text{(S41)}$$

Biological processes within the colony are parameterized similar to those in the single trichome model described above. Note that the light intensity in the colony [$I(t, r)$, μmol m^{-2} s^{-1}] is designed by multiplying $I(t)$ (*see* description about the trichome model above) with $\psi(r)$. Considering that there might be DIC limitation for carbon fixation of colony especially at the center, we introduced the parameter (η, dimensionless) to evaluate the strength of DIC limitation effect. η is regulated by the concentration of CO_2 and HCO_3^- in the microenvironment of colony:

$$\eta(r) = \min\left\{\frac{CO_2^M(r) + HCO_3^M(r)}{CO_{2,\,bsl}^E + HCO_{3,\,bsl}^E}, 1\right\}, \quad \text{(S42)}$$

where $HCO_{3,\ bsl}^{E}$ is the extracellular far-field HCO_3^- concentration (mol C m^{-3}). The carbon fixation of colony could be calculated based on ATP- and NADPH-dependent carbon fixation (*see* above) and η.

In the non-biological microenvironment of the colony, concentrations of O_2 [$O_2^M(r)$, mol O_2 m^{-3}], CO_2 [$CO_2^M(r)$, mol C m^{-3}], HCO_3^- [$HCO_3^M(r)$, mol C m^{-3}], CO_3^{2-} [$CO_3^M(r)$, mol C m^{-3}], H^+ [$H^M(r)$, mol H^+ m^{-3}], and OH^- [$OH^M(r)$, mol OH^- m^{-3}] are simulated at the radical distance r ($\leq R_C$). These concentrations are controlled by the physical diffusion, extracellular chemical reactions of carbonate system, and intracellular biological processes (e.g., net uptake or release). Therefore, their changing rates with time (t) and radical distance (r) can be represented using diffusion-reaction equations:

$$\frac{\partial O_2^M(r)}{\partial t}\cdot\psi(r)=\frac{1}{r^2}\cdot\frac{\partial}{\partial r}\left\{r^2\cdot[d_{O_2}\cdot\psi(r)]\cdot\frac{\partial O_2^M(r)}{\partial r}\right\}-T_{C,\ O_2}^{M}(r)\cdot[1-\psi(r)], \tag{S43}$$

$$\frac{\partial CO_2^M(r)}{\partial t}\cdot\psi(r)=\frac{1}{r^2}\cdot\frac{\partial}{\partial r}\left\{r^2\cdot[d_{CO_2}\cdot\psi(r)]\cdot\frac{\partial CO_2^M(r)}{\partial r}\right\}+J_{CO_2^M}(r)\cdot\psi(r)-T_{C,\ CO_2}^{M}(r)\cdot[1-\psi(r)], \tag{S44}$$

$$\frac{\partial HCO_3^M(r)}{\partial t}\cdot\psi(r)=\frac{1}{r^2}\cdot\frac{\partial}{\partial r}\left\{r^2\cdot[d_{HCO_3^-}\cdot\psi(r)]\cdot\frac{\partial HCO_3^M(r)}{\partial r}\right\}+J_{HCO_3^M}(r)\cdot\psi(r)-T_{C,\ HCO_3^-}^{M}(r)\cdot[1-\psi(r)], \tag{S45}$$

$$\frac{\partial CO_3^M(r)}{\partial t}\cdot\psi(r)=\frac{1}{r^2}\cdot\frac{\partial}{\partial r}\left\{r^2\cdot[d_{CO_3^{2-}}\cdot\psi(r)]\cdot\frac{\partial CO_3^M(r)}{\partial r}\right\}+J_{CO_3^M}(r)\cdot\psi(r), \tag{S46}$$

$$\frac{\partial H(r)}{\partial t}\cdot\psi(r)=\frac{1}{r^2}\cdot\frac{\partial}{\partial r}\left\{r^2\cdot[d_{H^+}\cdot\psi(r)]\cdot\frac{\partial H(r)}{\partial r}\right\}+J_{H^M}(r)\cdot\psi(r)-T_{C,\ H}^{M}(r)\cdot[1-\psi(r)], \tag{S47}$$

$$\frac{\partial OH(r)}{\partial t}\cdot\psi(r)=\frac{1}{r^2}\cdot\frac{\partial}{\partial r}\left\{r^2\cdot[d_{OH^-}\cdot\psi(r)]\cdot\frac{\partial OH(r)}{\partial r}\right\}+J_{OH^M}(r)\cdot\psi(r). \tag{S48}$$

where d_{O_2}, d_{CO_2}, $d_{HCO_3^-}$, d_{H^+} and d_{OH^-} are the diffusion coefficients of O_2, CO_2, HCO_3^-, H^+ and OH^- in seawater, respectively. Note that J represents the flux driven by driven by the chemical reactions in microenvironmental carbonate systems, and T denotes the flux interreacted with intracellular concentrations or processes, both of which are described later. M denotes the microenvironment.

The change rates of CO_2 [$J_{CO_2^M}(r)$, mol C m^{-3} s^{-1}], HCO_3^- [$J_{HCO_3^M}(r)$, mol C m^{-3}], CO_3^{2-} [$J_{CO_3^M}(r)$, mol C m^{-3}], H^+ [$J_{H^M}(r)$, mol H^+ m^{-3}], and OH^- [$J_{OH^M}(r)$, mol OH^- m^{-3}], driven by the chemical reactions in carbonate systems, are:

$$CO_2+H_2O\underset{k_{-1}}{\overset{k_{+1}}{\rightleftarrows}}HCO_3^-+H^+, \tag{S49}$$

$$CO_2 + OH^- \underset{k_{-4}}{\overset{k_{+4}}{\rightleftarrows}} HCO_3^-, \tag{S50}$$

$$CO_3^{2-} + H^+ \underset{k_{-5}}{\overset{k_{+5}}{\rightleftarrows}} HCO_3^-, \tag{S51}$$

$$H_2O \underset{k_{-6}}{\overset{k_{+6}}{\rightleftarrows}} H^+ + OH^-, \tag{S52}$$

$$J_{CO_2^M}(r) = [k_{-1} \cdot H^M(r) \cdot HCO_3^M(r) - k_{+1} \cdot CO_2^M(r)] + [k_{-4} \cdot HCO_3^M(r) - k_{+4} \cdot OH^M(r) \cdot CO_2^M(r)], \tag{S53}$$

$$\begin{aligned} J_{HCO_3^M}(r) = {} & [- k_{-1} \cdot H^M(r) \cdot HCO_3^M(r) + k_{+1} \cdot CO_2^M(r)] + [- k_{-4} \cdot HCO_3^M(r) + k_{+4} \cdot OH^M(r) \cdot CO_2^M(r)] \\ & + [k_{+5} \cdot H^M(r) \cdot CO_3^M(r) - k_{-5} \cdot HCO_3^M(r)]. \end{aligned} \tag{S54}$$

$$J_{CO_3^M}(r) = [k_{-5} \cdot HCO_3^M(r) - k_{+5} \cdot H^M(r) \cdot CO_3^M(r)], \tag{S55}$$

$$\begin{aligned} J_{H^M}(r) = {} & [- k_{-1} \cdot H^M(r) \cdot HCO_3^M(r) + k_{+1} \cdot CO_2^M(r)] + [k_{-5} \cdot HCO_3^M(r) - k_{+5} \cdot H^M(r) \cdot CO_3^M(r)] \\ & + [- k_{-6} \cdot H^M(r) \cdot OH^M(r) + k_{+6}], \end{aligned} \tag{S56}$$

$$J_{OH^M}(r) = [k_{-4} \cdot HCO_3^M(r) - k_{+4} \cdot OH^M(r) \cdot CO_2^M(r)] + [- k_{-6} \cdot H^M(r) \cdot OH^M(r) + k_{+6}], \tag{S57}$$

where k represents the reaction rate coefficient, and its subscript with positive or negative number represents the forward or reverse reaction, respectively.

The O_2 diffusion rate [$T^M_{C,\,O_2}(r)$, mol O_2 m^{-3} s^{-1}] between the intracellular cytoplasm and the extracellular microenvironment is:

$$T^M_{C,\,O_2}(r) = \frac{-2 \cdot \pi \cdot d_{O_2} \cdot L}{V} \cdot \left\{ \frac{1}{\varepsilon} \cdot \ln\left(\frac{R}{R + L_g} \right) \right\}^{-1} \cdot [O_2^M(r) - O_2(r)]. \tag{S58}$$

Considering the complexity of intracellular carbonate system with diffusion between cytoplasm and carboxysome, for simplification, the concentration of DIC and the reactions of carbonate system are not simulated in the intracellular cytoplasm as mentioned above. The exchange rates of CO_2 [$T^M_{C,\,CO_2}(r)$, mol C m^{-3} s^{-1}] was regulated by the CO_2 diffusion flux from microenvironment into cytoplasm [$\frac{\frac{-2 \cdot \pi \cdot d_{CO_2} \cdot L}{V} \cdot \left\{ \frac{1}{\varepsilon_{CO_2}} \cdot \ln\left(\frac{R}{R + L_g} \right) \right\}^{-1} \cdot CO_2^M(r)}{Q_C}$] and leakage flux into microenvironment [$(1 - f_{RP}^{CF}) \cdot V_{RP}(r)$]. The exchange rate of HCO_3^- [$T^M_{C,\,HCO_3^-}(r)$, mol C m^{-3} s^{-1}] was based on the requirement of HCO_3^- to support carbon fixation. The exchange rate of HCO_3^- [$T^M_{C,\,H}(r)$, mol H^+ m^{-3} s^{-1}] was the same as $T^M_{C,\,HCO_3^-}(r)$ [7]:

$$T^M_{C,\,CO_2}(r) = \frac{\frac{-2 \cdot \pi \cdot d_{CO_2} \cdot L}{V} \cdot \left\{ \frac{1}{\varepsilon_{CO_2}} \cdot \ln\left(\frac{R}{R + L_g} \right) \right\}^{-1} \cdot CO_2^M(r)}{Q_C} - (1 - f_{RP}^{CF}) \cdot V_{RP}(r), \tag{S59}$$

$$T^{M}_{C,\,HCO_3^-}(r) = V_{CF}(r) - f^{CF}_{RP} \cdot V_{RP}(r) - \frac{\frac{-2\cdot\pi\cdot d_{CO_2}\cdot L}{V} \cdot \left\{\frac{1}{\varepsilon_{CO_2}} \cdot \ln\left(\frac{R}{R+L_g}\right)\right\}^{-1} \cdot CO_2^M(r)}{Q_C}, \quad \text{(S60)}$$

$$T^{M}_{C,\,H}(r) = T^{M}_{C,\,HCO_3^-}(r). \quad \text{(S61)}$$

416

417 11. Model experiments with ammonia and copper toxicity

418 Ammonia (NH_3) and/or copper (Cu) toxicity can impact the response of the trichome to ocean
419 acidification [22]. Furthermore, previous study reported that the colony could also create a
420 chemical gradient of NH_4^+ and copper from the center to the edge [2,42]. Accordingly, we
421 conducted model experiments that incorporated the toxic effects of NH_3 and/or Cu into the
422 models for both trichome and colony.

423

424 Considering that NH_3 and/or Cu can inhibit photosystem II activity and photosynthetic ATP
425 production [22,43], we hypothesized that that NH_3 and/or Cu toxicity would negatively affect the
426 ATP production by the photosynthetic electron transfer chain. This effect (ξ, dimensionless) is
427 regulated by extracellular NH_3 and/or dissolved inorganic Cu concentration with pH level:

$$\xi = 1 - \frac{NH_3}{NH_3 + k_{NH_3}} \cdot \frac{Cu}{Cu + k_{Cu}} \cdot 10^{OA^{Cu}\cdot(pH - pH_{bsl})}, \quad \text{(S62)}$$

428 where $k_{NH_3} = 3\times10^{-5}$ mol N m^{-3} and $k_{Cu} = 2.5\times10^{-7}$ mol Cu m^{-3} are the half-saturating coefficient
429 of NH_3 and Cu concentrations for the toxic effect, and $OA^{Cu} = 1.65$ represents the strength of
430 negative effect from acidification on copper availability.

431

432 The concentration of NH_3 was calculated based on the pH level, NH_4^+ concentration, and the
433 equilibrium constant for the chemical reaction between NH_3 and NH_4^+. In the colony model,
434 microenvironmental NH_4^+ concentration profile was predefined according to the findings of
435 Klawonn, et al. [2]. The pattern of microenvironmental Cu was set the same as that of NH_4^+, with
436 the highest concentration (1 nmol L^{-1}) at the center of the colony. This concentration selection is
437 supported by observations from Wang, et al. [42].

438

439 Given an approximate colony volume of ~1 μL, dust loads of 0.2–1 μg per colony yield an
440 effective dust concentration of 200–1,000 mg/L [42]. In situ observations of puff-shaped colonies
441 indicate that each colony typically contains less than 200 ng of dust, corresponding to ~200 mg/L
442 [42]. Based on these estimations and relationship between dust and Cu concentrations [42], a Cu

443 concentration of 1 nmol L^{-1} could be considered a conservative estimate. Additionally,
444 observations of trichome growth in YBC-II media with 1 nmol L^{-1} Cu have likely demonstrated
445 toxic effects [22], further supporting the relevance of this concentration for the colony model
446 experiments.
447

SUPPLEMENTAL REFERENCES

1. Luo, Y.W. *et al.* Reduced nitrogenase efficiency dominates response of the globally important nitrogen fixer *Trichodesmium* to ocean acidification. *Nature Communications* **10**, 1521 (2019).
2. Klawonn, I. *et al.* Distinct nitrogen cycling and steep chemical gradients in *Trichodesmium* colonies. *The ISME Journal* **14**, 399-412 (2020).
3. Luo, W. & Luo, Y.-W. Diurnally dynamic iron allocation promotes N_2 fixation in marine dominant diazotroph *Trichodesmium*. *Computational and Structural Biotechnology Journal* **21**, 3503-3512 (2023).
4. Luo, W., Inomura, K., Zhang, H. & Luo, Y.-W. N_2 fixation in *Trichodesmium* does not require spatial segregation from photosynthesis. *mSystems* **7**, e00538-22 (2022).
5. Inomura, K., Wilson, S.T. & Deutsch, C. Mechanistic model for the coexistence of nitrogen fixation and photosynthesis in marine *Trichodesmium*. *mSystems* **4**, e00210-19 (2019).
6. Benson, B.B. & Krause, D. The concentration and isotopic fractionation of oxygen dissolved in freshwater and seawater in equilibrium with the atmosphere. *Limnology and Oceanography* **29**, 620-632 (1984).
7. Wolf-Gladrow, D. & Riebesell, U. Diffusion and reactions in the vicinity of plankton: A refined model for inorganic carbon transport. *Marine Chemistry* **59**, 17-34 (1997).
8. Allen, J.F. Cyclic, pseudocyclic and noncyclic photophosphorylation: New links in the chain. *Trends in Plant Science* **8**, 15-19 (2003).
9. Geider, R.J., Moore, C.M. & Ross, O.N. The role of cost–benefit analysis in models of phytoplankton growth and acclimation. *Plant Ecology and Diversity* **2**, 165-178 (2009).
10. Flores, E. & Herrero, A. Assimilatory nitrogen metabolism and its regulation. in *The Molecular Biology of Cyanobacteria* (ed. Bryant, D.A.) 487-517 (Kluwer Academic Publishers, Dordrecht, 1994).
11. Flores, E., Frías, J.E., Rubio, L.M. & Herrero, A. Photosynthetic nitrate assimilation in cyanobacteria. *Photosynthesis Research* **83**, 117-133 (2005).
12. Baker, N.R., Harbinson, J. & Kramer, D.M. Determining the limitations and regulation of photosynthetic energy transduction in leaves. *Plant Cell and Environment* **30**, 1107-1125 (2007).
13. Raven, J.A., Beardall, J. & Giordano, M. Energy costs of carbon dioxide concentrating mechanisms in aquatic organisms. *Photosynthesis Research* **121**, 111-124 (2014).
14. Mitchell, P. Aspects of the chemiosmotic hypothesis. *Biochemical Journal* **116**, 5-6 (1970).
15. Bratbak, G. & Dundas, I. Bacterial dry matter content and biomass estimations. *Applied and Environmental Microbiology* **48**, 755-757 (1984).
16. Carpenter, E.J. *et al.* The tropical diazotrophic phytoplankter *Trichodesmium*: Biological characteristics of two common species. *Marine Ecology Progress Series* **95**, 295-304 (1993).
17. LaRoche, J. & Breitbarth, E. Importance of the diazotrophs as a source of new nitrogen in the ocean. *Journal of Sea Research* **53**, 67-91 (2005).
18. Shi, D., Kranz, S.A., Kim, J.M. & Morel, F.M. Ocean acidification slows nitrogen fixation and growth in the dominant diazotroph *Trichodesmium* under low-iron conditions. *Proceedings of the National Academy of Sciences of the United States of America* **109**, E3094-100 (2012).
19. Shao, Z. *et al.* Global oceanic diazotroph database version 2 and elevated estimate of global oceanic N_2 fixation. *Earth System Science Data* **15**, 3673-3709 (2023).

20. Capone, D.G., Zehr, J.P., Paerl, H.W., Bergman, B. & Carpenter, E.J. *Trichodesmium*, a globally significant marine cyanobacterium. *Science* **276**, 1221-1229 (1997).
21. Chen, Y.B., Dominic, B., Mellon, M.T. & Zehr, J.P. Circadian rhythm of nitrogenase gene expression in the diazotrophic filamentous nonheterocystous cyanobacterium *Trichodesmium* sp. strain IMS 101. *Journal of Bacteriology* **180**, 3598-3605 (1998).
22. Hong, H. *et al.* The complex effects of ocean acidification on the prominent N_2-fixing cyanobacterium *Trichodesmium*. *Science* **356**, 527-531 (2017).
23. Shi, D., Shen, R., Kranz, S.A., Morel, F.M.M. & Hong, H. Response to Comment on "The complex effects of ocean acidification on the prominent N_2-fixing cyanobacterium *Trichodesmium*". *Science* **357**(2017).
24. Reimers, A.M., Knoop, H., Bockmayr, A. & Steuer, R. Cellular trade-offs and optimal resource allocation during cyanobacterial diurnal growth. *Proceedings of the National Academy of Sciences of the United States of America* **114**, E6457-E6465 (2017).
25. Milligan, A.J., Berman-Frank, I., Gerchman, Y., Dismukes, G.C. & Falkowski, P.G. Light-dependent oxygen consumption in nitrogen-fixing cyanobacteria plays a key role in nitrogenase protection. *Journal of Phycology* **43**, 845-852 (2007).
26. Behrenfeld, M.J. & Milligan, A.J. Photophysiological expressions of iron stress in phytoplankton. *Annual Review of Marine Science* **5**, 217-246 (2013).
27. Berman-Frank, I. *et al.* Segregation of nitrogen fixation and oxygenic photosynthesis in the marine cyanobacterium *Trichodesmium*. *Science* **294**, 1534-1537 (2001).
28. Gallon, J.R. The oxygen sensitivity of nitrogenase: A problem for biochemists and micro-organisms. *Trends In Biochemical Sciences* **6**, 19-23 (1981).
29. Hutchins, D.A. *et al.* CO_2 control of *Trichodesmium* N_2 fixation, photosynthesis, growth rates, and elemental ratios: Implications for past, present, and future ocean biogeochemistry. *Limnology and Oceanography* **52**, 1293-1304 (2007).
30. Eichner, M., Kranz, S.A. & Rost, B. Combined effects of different CO_2 levels and N sources on the diazotrophic cyanobacterium *Trichodesmium*. *Physiologia Plantarum* **152**, 316-330 (2014).
31. Levitan, O. *et al.* Elevated CO_2 enhances nitrogen fixation and growth in the marine cyanobacterium *Trichodesmium*. *Global Change Biology* **13**, 531-538 (2007).
32. Kranz, S.A., Sültemeyer, D., Richter, K.-U. & Rost, B. Carbon acquisition by *Trichodesmium*: The effect of pCO_2 and diurnal changes. *Limnology and Oceanography* **54**, 548–559 (2009).
33. Barcelos e Ramos, J., Biswas, H., Schulz, K.G., LaRoche, J. & Riebesell, U. Effect of rising atmospheric carbon dioxide on the marine nitrogen fixer *Trichodesmium*. *Global Biogeochemical Cycles* **21**, GB2028 (2007).
34. Inomura, K. *et al.* Quantifying oxygen management and temperature and light dependencies of nitrogen fixation by *Crocosphaera watsonii*. *mSphere* **4**, e00531-19 (2019).
35. Staal, M., Meysman, F.J. & Stal, L.J. Temperature excludes N_2-fixing heterocystous cyanobacteria in the tropical oceans. *Nature* **425**, 504-507 (2003).
36. Kustka, A.B. *et al.* Iron requirements for dinitrogen‐ and ammonium‐supported growth in cultures of *Trichodesmium* (IMS 101): Comparison with nitrogen fixation rates and iron: carbon ratios of field populations. *Limnology and Oceanography* **48**, 1869–1884 (2003).
37. Berman-Frank, I., Cullen, J.T., Shaked, Y., Sherrell, R.M. & Falkowski, P.G. Iron availability, cellular iron quotas, and nitrogen fixation in *Trichodesmium*. *Limnology and*

Oceanography **46**, 1249-1260 (2001).
38. Capone, D.G., O'Neil, J.M., Zehr, J.P. & Carpenter, E.J. Basis for diel variation in nitrogenase activity in the marine planktonic cyanobacterium *Trichodesmium thiebautii*. *Applied and Environmental Microbiology* **56**, 3532-3536 (1990).
39. Shampine, L.F. & Reichelt, M.W. The MATLAB ODE Suite. *SIAM J Sci Comput* **18**, 1-22 (1997).
40. Finzi-Hart, J.A. *et al.* Fixation and fate of C and N in the cyanobacterium *Trichodesmium* using nanometer-scale secondary ion mass spectrometry. *Proceedings of the National Academy of Sciences of the United States of America* **106**, 6345-6350 (2009).
41. Shi, T., Sun, Y. & Falkowski, P.G. Effects of iron limitation on the expression of metabolic genes in the marine cyanobacterium *Trichodesmium erythraeum* IMS101. *Environmental Microbiology* **9**, 2945-56 (2007).
42. Wang, S. *et al.* Costs of Dust Collection by *Trichodesmium*: Effect on Buoyancy and Toxic Metal Release. *Journal of Geophysical Research: Biogeosciences* **129**, e2023JG007954 (2024).
43. Cid, A., Herrero, C., Torres, E. & Abalde, J. Copper toxicity on the marine microalga *Phaeodactylum tricornutum*: effects on photosynthesis and related parameters. *Aquatic Toxicology* **31**, 165-174 (1995).